Master's thesis

NTNU
Norwegian University of Science and Technology

Tina Vincens Sørensen, Radiographer, Dept. of Radiology, Odense Universitets Hospital, Denmark

Metal Artifact Reduction for Total Hip Replacement in MRI

Optimizing a metal artifact reducing sequence protocol

Master's thesis in Master i medisinsk MR-avbildning
Supervisor: Professor Henrik Bo Larsson, Functional Imaging Unit, Dept. of Clinical Physiology, Nuclear Medicine & PET, Rigshospitalet, Glostrup, Denmark

December 2019

NTNU
Norwegian University of Science and Technology

Tina Vincens Sørensen, Radiographer, Dept. of Radiology, Odense Universitets Hospital, Denmark

Metal Artifact Reduction for Total Hip Replacement in MRI

Optimizing a metal artifact reducing sequence protocol

Master's thesis in Master i medisinsk MR-avbildning
Supervisor: Professor Henrik Bo Larsson, Functional Imaging Unit, Dept. of Clinical Physiology, Nuclear Medicine & PET, Rigshospitalet, Glostrup, Denmark
December 2019

Norwegian University of Science and Technology

NTNU
Norwegian University of Science and Technology

Metal artifact reduction for total hip replacement in MRI

Optimizing a metal artifact reducing sequence protocol

Radiographer: Tina Vincens Sørensen, Odense University Hospital, Denmark
Supervisor: Professor Henrik Bo Larsson, Functional Imaging Unit, Dept. of Clinical Physiology, Nuclear Medicine & PET, Rigshospitalet, Glostrup, Denmark, Department of Circulation and Medical Imaging, NTNU, Norway
| Masteropgave NTNU | 15.12.2019

TABLE OF CONTENTS

1. Introduction

Magnetic Resonance Imaging (MRI) is the preferred imaging modality in many clinical situations, where there is a necessity to visualize anatomy and pathology. Unlike conventional radiography images, computed tomography imaging, scintigraphy or positron emission tomography, MRI enables visualization of the soft tissue adjacent to the metal hip implants. (1) The implants still cause diagnostic difficulties using MRI and therefor applying metal artifact reducing sequences (MARS) are attempts of optimizing the images.

Patients that have discomfort and pain from their hip arthroplasty can be referred to an MRI scan. The radiologist may suspect pseudo tumors close to the metal hip. Diagnosing pseudotumor can require MRI as the primary image modality. The initial step is a blood test, that provides insight into whether there is an increase of metal ions in the patients' bloodstream. The causality between pseudo tumors and Metal on Metal prostheses (MoM) is not clear. (2)

1.1 Background

Following a scanner upgrade of both hardware and software at the radiology department, the necessity for revising protocols was quickly apparent. The need to find the best solution of artifact reducing sequences that will contribute to optimized image quality around total hip arthroplasty (THA) at 1.5T was favored. MRI of the hips are usually scanned at 3T, but as higher field strength increases susceptibility artifacts, the image quality there was significantly reduced around the THA. (3)

The existing metal artifact reduction protocol could consist of inadequate or obsolete image sequences, as there has not been protocol revision in some time. The initial Orthopedic Metal Artifact Reduction sequence (OMAR) was the golden standard previously when applying Metal Artifact Reducing Sequences (MARS) techniques. The newer OMAR sequences (OMAR XD) has been recommended by manufactures. This project could provide deeper insight into the sequence's strengths and weaknesses for both OMAR and OMAR XD.

MRI manufacturers offer dedicated metal artifact reduced techniques that include high bandwidth optimization, View Angle Tilting (VAT) and Slice-Encoding for Metal Artifact Correction (SEMAC). These techniques should reduce the metal artifacts significantly, but this is acquired at the expense of SNR, increased SAR and prolonged scan time. (3)

When assessing images with metal implants as figure 1, it is apparent that the possibility of visualizing the anatomy and pathology in the metal-related area are challenging. This is the reason for implementing this scientific study for the knowledge and thereby optimizing the existing available protocol with a better and more suited version. The benefits could be a new protocol with VAT and SEMAC sequences applied more efficient that the existing protocol.

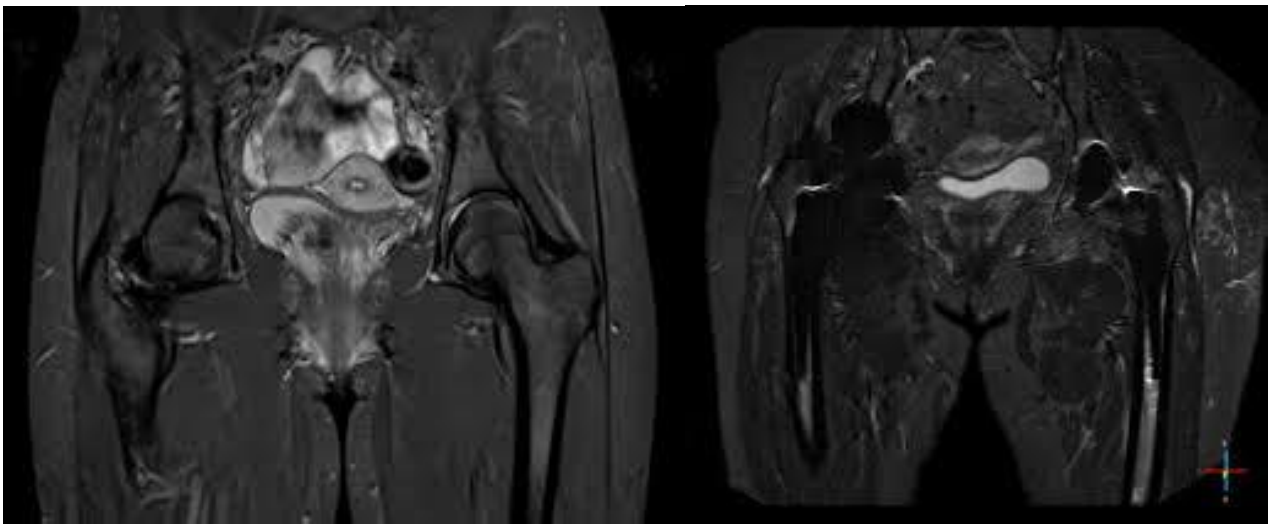

Figure 1 shows on the left (4) a coronal image of the hips and on the right (5) the same orientation and anatomy, with bilateral metal hip implants. Both images are a STIR sequence.

1.2 The aim and purpose

The aim of the phantom study is to optimize the existing protocol for THA scans using OMAR and OMAR XD sequences. Another objective was optimizing these sequences so they can be implemented in the routine THA scans performed on a regular basis in the department. The next part of the study could be determining whether the new sequences will be better than the golden standard protocol by scanning a healthy volunteer.

The primary purpose is to compare the golden standard pseudo tumor protocol consisting of Philips MARS sequences (OMAR and OMAR XD) to optimized sequences in order to reduce artifacts near two different THA models as a phantom study.

The secondary purpose is to compare and adjust the artifact reduction protocol by scanning the volunteer that has an arthroplasty with the golden standard- and the new optimized protocol.

1.3 Concept operationalization

OMAR: Orthopedic Metal Artifact Reduction is the combination of MARS with VAT technique. VAT is an applied technic that correct for artifacts in the in-plane direction. (6)

OMAR XD: This technique combines SEMAC with the VAT method. By applying both methods, the susceptibility artifact reduction will be reduced in both in-plane and through-plane directions. (6)

THA: Total Hip Arthroplasty is a metallic replacement joint, consisting of both femoral head (caput femur) and the femoral neck (collum femur). There are numerous prosthetic hip components available. Hip-TC consists of a titanium stem and cup in conjunction with a ceramic head. This is the most commonly used hip implant that subsequently produce a minimal MRI artifact. Hip-MM consists of a titanium stem with a Cobolt Chromium (CoCr) cup and head. This is the most commonly used metal-on-metal hip implant and produce the largest femoral head artifact. Hip-SOPC is an older type of hip implant consisting of a stainless-steel stem, with a Polyethylene and CoCr cup and an Oxinium femoral head. (6)

1.4 Description of pseudotumor

The first documented pseudo tumor was in 1976 as an aggressive granulomatous lesion connected to a cemented THA with metal polyethylene articulation. The cause for inflammatory pseudo tumors is not known. Imaging these pseudo tumors is often difficult. A blood test with increased ion can be an indication for the presence of pseudo tumors. (2) The pseudotumor is mentioned in both hip- and knee arthroplasties with both metal/polyethylene and Metal-on-Metal articulations. The pseudotumor is defined as a granulomatous or destructive cystic or solid lesion. It is not an infectious nor is it neoplastic in nature, but it develops near the THA. A blood test with cobalt (Co) and chromium (Cr) levels of 7 ppb as a threshold. (7,8)

The pseudotumors produce a hypersensitive reaction because of the prosthesis, where the soft tissue is affected, along with periprosthetic cystic, solid or mixed masses that can further along lead to necrosis and long-term complications. These complications can develop shortly after the THA surgery or years later. Symptoms are not specific and not always present for the patient. The symptoms can be pain, joint instability and the presence of palpable masses. The detection of increased chromium and cobalt is measured from the blood, in the patients urine or extracting joint fluid. (9)

2. Theory

Metal artifact reduction has been approached using different strategies in other studies. It is not recommended to use parallel imaging techniques such as SENSE as this reduces SNR further, where enough signal is required in the presence of metal in the area. The geometric distortion of metal close areas is caused by "error" in the Larmor frequencies. It is useful to work with an increased bandwidth. By increasing receiver bandwidth, the chemical shift artifacts will be reduced, which is relevant when water-fat shift is reduced. This means that there is a markedly smaller geometric distortion in the in-plane of the FoV. It is also possible to use thinner slices that will decrease SNR around the metal implant. However, as there is still signal loss, you can benefit from increasing the NSA, which increases the scan time. (10) It is not always obvious which MARS technology is considered suitable for optimal image assessment surrounding a THA as the human factor is present.

2.1 Metal artifact

The introduction of metal in the scanner leads to variations in the static magnetic field, superimposing all imaging gradients which results in through-plane artifact. This is because of the corruption of the slice selection gradient. Furthermore, there will be in-plane artifact present in the images, due to the corruption of the frequency encoding gradient. Displacement artifacts occur in the slice selection as well as the in the frequency direction. The resulting metal artifact image will have curved, thickened, thinned or split slice, that is viewed as signal loss, signal pile-up and geometric distortion in the image. (11) The signal loss in the image produces a drop in SNR, resulting in a range of noisy image to total signal void. The signal pile-up is viewed as a curvilinear hyperintense signal that follows the prosthesis' curvature and is near the signal void area. The distortion in the MR image is causes warping of the normal THA contour. These three aspects is worsened with higher field strength, ferromagnetic alloys instead of titanium and spherical prostheses rather than linear solutions. (12) The degree of distortion in the MR image depends on the different metallic components in the THA and the choice of artifact reducing sequence used.

2.1.1 Magnetic susceptibility

There is a close relationship between susceptibility and metal artifacts. The differences in tissue, due to microscopic field changes, when introduced to the MR scanner. The protons have in increased

dephasing around the borders between two different tissues, where the signal intensity of the voxels is reduced in the specific area. The metals introduced to the body have a significant higher susceptibility than the protons in tissue creating large magnetic field inhomogeneities around the object. (13)

The magnetic susceptibility is a dimensionless constant (X) that indicate the degree of how magnetized (M) a material becomes when it is applied in a magnetic field (H). This is defined by the following equation: $X=M/H$. (14)

X is expressed in parts per million (ppm), M and H are measured in amperes per meter (A/m). Diamagnetism has a magnetic susceptibility of $X<0$ ppm, where paramagnetism has susceptibility of $0<X<300$ ppm and ferromagnetism have a susceptibility $X>300$ ppm. Table 1 shows some of the susceptibility differences between tissues, air and metals. (14)

Table 1 Magnetic susceptibility in tissue and materials along with their magnetism. (14)

Material	Magnetic susceptibility (ppm)	Magnetism
Water (soft tissue)	−9.05	Diamagnetism
Cortical bone	−8.86	
Liver	−8.76	
Blood (deoxygenated)	−7.9	
Liver (hemochromatosis)	0	
Air	0.36	Paramagnetism
Aluminium	20.7	
Titanium	182	
Gadolinium contrast agent (0.1 mol/l)	249	
Chromium-cobalt	900	Ferromagnetism

Arthroplasties are placed along with gadolinium in the paramagnetic area of the magnetic susceptibility spectrum, when they consist of titanium. When they consist of stainless steel, the arthroplasty is on the border between para-, and ferro-magnetic spectrum. See Appendix (8). (15)

2.1.2 Chemical shift

During the standard pulse sequence, the frequency-encoding occurs after the phase-encoding, right before the MR signal is acquired. During the slice selection, there is a marginally offset between the location of the two different tissues. During the phase encoding gradient two tissues acquire phase at

different rates, when compared to each other. This results in these two tissues in the same voxel are encoded as being positioned in different voxels. When then phase encoding gradient is applied, the spins at different positions precess at a frequency corresponding to their own Larmor frequency. After turning of the phase encoding gradient, each vector has developed a unique phase, that is dependent on its position. (16) The frequency-encoding delivers the spatial information one direction of the image. Tissues like fat have a lower frequency than water. Therefore, a pixel shift in the frequency-encoding direction will happen. The effects of this shift occur because the fat and water spins in the same voxel, are encoded but interpreted in different voxels. This chemical shift can be severe if the receiver bandwidth is too low. One of the downsides of high bandwidth is a reduction in signal-to-noise ratio (SNR). Chemical shift between fat and water is 3,5 ppm at 1,5T. (13)

The precessional frequency difference of the proton in fat and water is 220Hz for a 1.5T scanner, which is shown below:

Frequency = $\omega_0 = \gamma B_0$; => (42,6 MHz/T) (1.5T) = $64*10^6$ Hz

3.5 ppm = $3,5*10^{-6}$

$(3.5*10^{-6})$ $(64*10^6)$ = 220Hz (17)

Chemical shift artifacts are primarily visualized along the frequency encoding direction. (18)

2.1.3 Water-fat shift

The chemical shift is the difference in frequency and is field strength dependent. At 1.5T the difference between fat and water is 220Hz, as shown in the previous segment. This shifts in position occurs in the frequency direction. This water-fat shift (WFS) is the displacement of the water signal compared to the fat signal and can be expressed in number of pixels. Table 2 is an informational tool to use in optimizing a scan. (19)

Table 2 show possibilities of optimizing MR sequences in regard to WFS and bandwidth. (19)

Water-fat shift	Bandwidth
Reduce water-fat shift to reduce chemical shift artifacts	**Increase bandwidth** to reduce chemical shift artifacts
Reduce water-fat shift to reduce metal artifacts	**Increase bandwidth** to reduce metal artifacts
Increased water-fat shift increases SNR	**Narrowing bandwidth** increases SNR
Reduce water-fat shift to reduce readout duration and echo spacing, and limit blurring	**Increase bandwidth** to reduce readout duration and echo spacing, and limit blurring

The Philips scanner advises the user of, what the consequences are when reducing WFS and the equivalent bandwidths countermeasures.

2.2 MRI Parameters

There are several parameters that can aid and hinder the reduction of artifacts in the MR image. The task is to try to control the two types of geometric distortion. The in-plane distortions are caused by the disrupted frequency encoding when the signal readout is occurring. These distortions are signal loss and pileup artifacts. The other is through-plane distortion, which is the result of a distorted excitation profile during the slice selective excitation. This type of distortion arises from local field inhomogeneities due to the ferromagnetic properties caused by the material implanted. (20)

Before addressing different sequences as OMAR and OMAR XD, the foundation of artifact reduction will be mentioned.

2.2.1 Bandwidth

The receiver bandwidth has a direct correlation to SNR and depends on frequency encoding, the gradients strength and the data samplings rate. One way of reducing the in-plane artifacts is by increasing the read-out bandwidth. When strong gradients are applied, the voxels are each encoded by a wider range of frequencies. Strong gradients are required to manage a doubling of bandwidth to usual sequences. The SNR will be markedly reduced with this increased bandwidth adjustment. Scan averages (NSA) may need to be increased in order to receive enough signal which results in increased scan time. With an increase in bandwidth, the echo spacing can be reduced, resulting in less T_2 decay along with less signal loss. The SAR will be increased as a result of this application. The requirements for each chosen bandwidth are based upon the degree for chemical shift, the amount of SNR and the minimum echo time. Chemical shift artifacts are the mismatch of off-resonant spins that happen when the frequency encoding is applied for spatial positioning and selection. Other displacements can occur with spatial magnetic susceptibility or B_0 inhomogeneity. The artifacts due to chemical shift happen in the read-out-, slice-selection- or slice encoding direction for most pulse sequences. (21)

The cause for the chemical shift in the read-out direction is visualized in figure 2. The frequency-encoding gradient creates a varying precession frequency across the FOV. In the figure 2 below, the frequency encoding gradient has a varied precession frequency across the FoV in the linear direction. The spin precession at x_1 with the frequency f_1 is on-resonance. At x_2 with frequency f_2 the spin is off resonance.

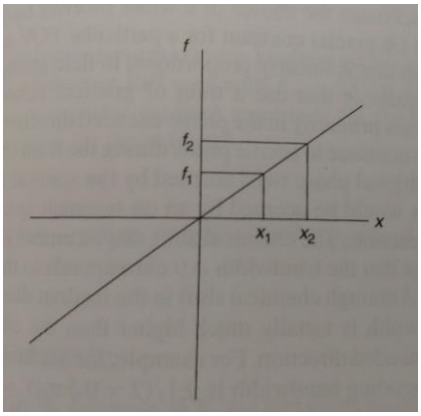

Figure 2 shows the differences between on-, and off-resonance images due to the difference in frequency. (31)

The difference between the X-axis values of the on- and off-resonance is the shift distance $\delta x = x_2 - x_1$, given by Eq.1:

$$\delta z = \frac{2\pi\delta f}{\gamma G} \quad (1)$$

$\delta f = f_2 - f_1$ is the displacement of frequency. The chemical shift displacement is calculated by Eq.2:

$$\Delta x_{FoV/x\_FoV} = \frac{\delta x}{Lx} = \frac{\delta f}{2\Delta\nu} \quad (2)$$

The shift in pixels across the FoV is seen in Eq.3:

$$\delta x_{pixel} = \frac{Nx\delta x}{Lx} = \frac{Nx\delta f}{2\Delta\nu} \quad (3)$$

Lx is the FoV, Nx is the readout point and $2\Delta\nu$ is full bandwidth. This shift distance can be minimized with an increase in bandwidth. By doing this the SNR will as a result be reduced. The increased or reduced chemical shift is also depended on the B_0-field strength. At high magnetic field strengths (1,5T or 3T) a wide receiver bandwidth of ex. 16000Hz is a necessity for reduced chemical shift and magnetic susceptibility artifacts. (31)

By introducing higher bandwidth, this will reduce signal misregistration in the in-plane frequency encoding direction. With this approach, the shift of spins with wrong frequency is reduced. (3) Guide lines for an estimated value of an acceptable bandwidth is viewed greater than 500Hz/pixel. (14) The SNR and contrast information is found in the lower RF frequencies. By using the higher bandwidth, chemical shift artifacts will be reduced. (13)

2.2.2 Matrix

The spatial resolution is defined by the imaging voxels. The voxel size and image resolution depend on the matrix size, the field of view (FoV) and the thickness of the slices. The matrix makeup is the number of frequency encoding steps in one direction (often the larger value depicted on the matrix size), and the number of phase encoding steps in the other direction (often the smaller number viewed on the scanner display). (22) In an attempt of increasing the image resolution, the matrix size is increased for in-plane artifact reduction. This reduces both in-plane distortion and intravoxel dephasing. A matrix size of 512 is preferable and performed in the frequency encoding direction. (3)

2.2.3 Signal-to-Noise Ratio and Contrast-to-Noise Ratio

The SNR is defined as $\frac{signal}{noise} = SNR$. The viewed MR image voxel will contain a mixture of both signal and noise. A poor SNR will result in a fuzzy and un-sharp image. There are different options to increase SNR. The easiest way is an increase in NSA that result in an increased scan time. If this is not an option, it is possible to increase the slice thickness or increased the FoV. SNR measurements are produced by applying a region of interest (ROI) within the phantom, where 75% of the phantom is included. Eq.4 shows the calculation of SNR.

$$SNR = \frac{0{,}665 * mean\ signal}{average\ of\ noise\ region\ standard\ deviations} \quad (4)$$

0,665 is a factor for Rayleigh distribution correction and resulting in Eq.5.

$$SNR = \frac{0{,}665 * S}{\sigma}. (13) \quad (5)$$

Contrast-to-noise ratio (CNR) is viewed in tissues, where two different tissues are subtracted from each other and that sum is then divided by the surrounding noise, and viewed in Eq.6.

$$\frac{Tissue1-Tissue2}{noise} = CNR. \text{ (13)} \quad (6)$$

2.2.4 Echo Spacing

The number of echoes produced after the application of the RF pulse is the echo train length. (21) With the usage of turbo spin echo sequences, the number of echoes or turbo factor is introduced along with the time between echoes, called echo spacing (ESP). The turbo factor is an important parameter when adjusting a sequence. A long turbo factor results in more T2W due to the late echoes with longer TE's that contribute to the combined signal. By doing so, the SNR and CNR will decrease in general, because the later echoes get weaker and weaker. An increase in ESP will give the advantage of longer TE's but also impacts SNR and CNR. It is better to apply the shortest permitted ESP. (23)

2.2.5 Slice thickness

The resolution is related to the acquired FoV, acquisition matrix and slice thickness. The size of the pixel (FoV/matrix) determines the in-plane resolution. Smaller voxels produce high spatial resolution but low SNR. The slice thickness provides the depth of the voxel. (24)

It is preferable to reduce the slice thickness, by introducing a strong slice selection gradient, that aids in reducing through-plane distortion. Slice thickness can range, but for hip sequences 3-4 millimeters are sought after. Having thinner slices will improve artifact reduction. It is possible to reduce the through-plane artifacts by reducing the slice selection bandwidth, resulting in an increased scan time and the SNR will be reduced. It is possible to adjust the slice thickness bandwidth. This is not a user-accessible function because it consists of enlarging the RF bandwidth. (3,14)

2.2.6 View Angle Tilting

A conventional SE image is shown in figure 3 consisting of bone and metal on the left side. View-angle tilting (VAT) is applied on the right side.

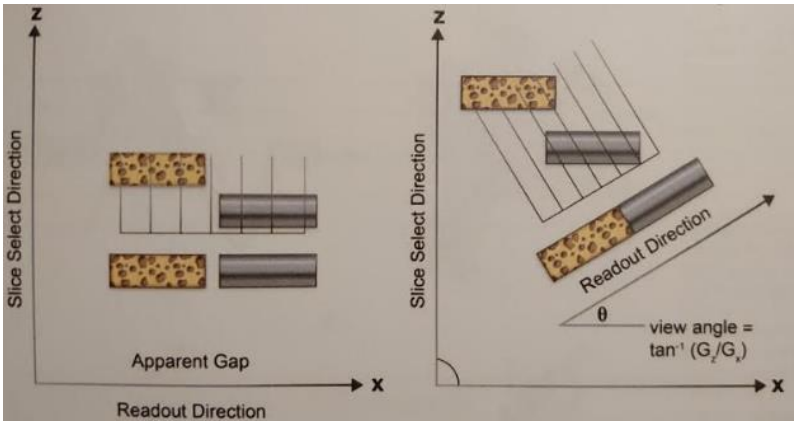

Figure 3 shows the conventional MR imaging on the left. On the right VAT minimizes the in-plane distortion, by adding an altered readout gradient at angle θ. This results in reduced signal loss and pile-up artifacts, but with a sight blurring. (25)

VAT reduces in-plane metal artifact distortion and is applied during signal readout as an additional slice-selection gradient at the same time as the sequence's read-out gradient. (25) Thus, the "tilt" read encoding against the slice selection dimension with which all off-resonance causes displacements along the read-out direction and is removed in the excised section. Due to the "tilting" there appears to be blurring in the image, seen on the right in figure 4. To reduce the blurring that VAT increases, thin slices and increased readout bandwidth is a necessity. The trade-off is reduced SNR. (3,14,26)

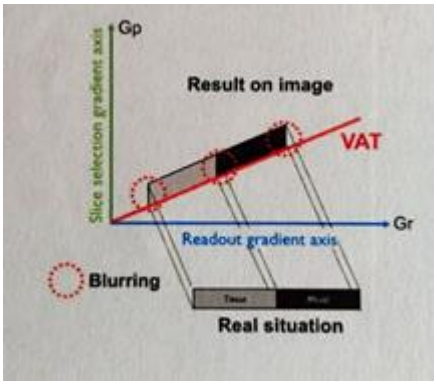

Figure 4 shows the VAT method resulting in blurring between tissue and metal. (14)

VAT is not able to remove the distortion that occurs perpendicular to the image plan. Furthermore, VAT can induce some blurring caused by the geometrical tilting of the image pixels, and by the low pass filter superimposing on the read-out signal. The blurring caused by the low pass filtering results in a loss of image detail, whereas the tilting effect is mostly visible at the edge of the anatomy and more obvious when the section thickness is increased. (27)

2.3 MRI Sequences

The susceptibility artifacts from metal have always irritated users and the battle for producing usable images has been present for years. Initially the simple changes were using lower field strength, prioritizing spin echo sequences as opposed to gradient echo sequences and using short tau inversion recovery (STIR) instead of fat suppression. (28,29)

Philips' two metal artifact reducing sequences are OMAR a combination of MARS and VAT technique and OMAR XD that combines the SEMAC with the VAT method. (6)

2.3.1 OMAR

The sequence consists of high-bandwidth turbo spin echo with VAT. A standard T1W coronal sequence of the hip has a bandwidth of approximately 745 Hz/pixel, water-fat-shift of about 0,3 pixels, with slice thickness of 3 mm. and applying 2 NSA. The in-plane frequency encoding is performed right to left. The matrix size is 300*257, a voxel size of 0.52*0.52mm, a turbo factor of 5 and a scan time of 4:51 min. (Philips Inginia dStream 1.5T) Most of the technical advances have been attempted to obtain the best quality with this sequence. The receiver bandwidth (BW=N/Ts) is the reciprocal of the total sampling time (Ts) times N, which is matrix in the read(N) * dwell time(D) = Ts. By increasing the bandwidth, the sampling time will be shortened i.e. Ts is decreased. It will reduce the signal amplitude and increase the noise level in the pixels, that visibly reduces the SNR. (30)

By applying VAT to the high bandwidth turbo spin echo (TSE) sequence, VAT takes advantage of the displacement of the slice and in-plane displacement since off-resonance have a constant ratio. VAT replays the slice selection gradient during the readout, which then angles the image plane of the slice and readout direction. (31) This is seen in figure 5. The in-plane distortion occurs along the read-out direction (x plane) and seen as Δx with the through-plane displacement Δz occurs along the slice-selection (z plane). The angle of displacement is φ. With the VAT there will be blurring from the pixel shearing, that it the area where the two tissues meet. (32)

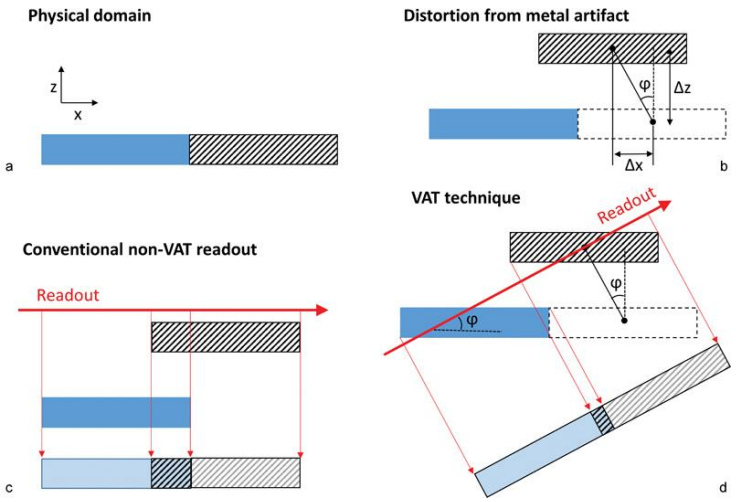

Figure 5 shows four parts, with two blocks close together in physical domain (a). The blue/solid block is not influenced by the metal-induced magnetic field variation but the block next to it consists of off-resonance spins that now are displaced in a new position (b). In a conventional sequence without VAT (c), the read-out in the x direction shows the in-plane artifacts by the overlay of the two blocks. By introduction VAT (d), the slice-selection gradient is replayed at the same time as signal acquisition that tilts the read-out direction at the angle φ. (32)

Viewing the differences between low bandwidth, higher bandwidth and the presence of VAT in the MR image can be seen in figure 6.

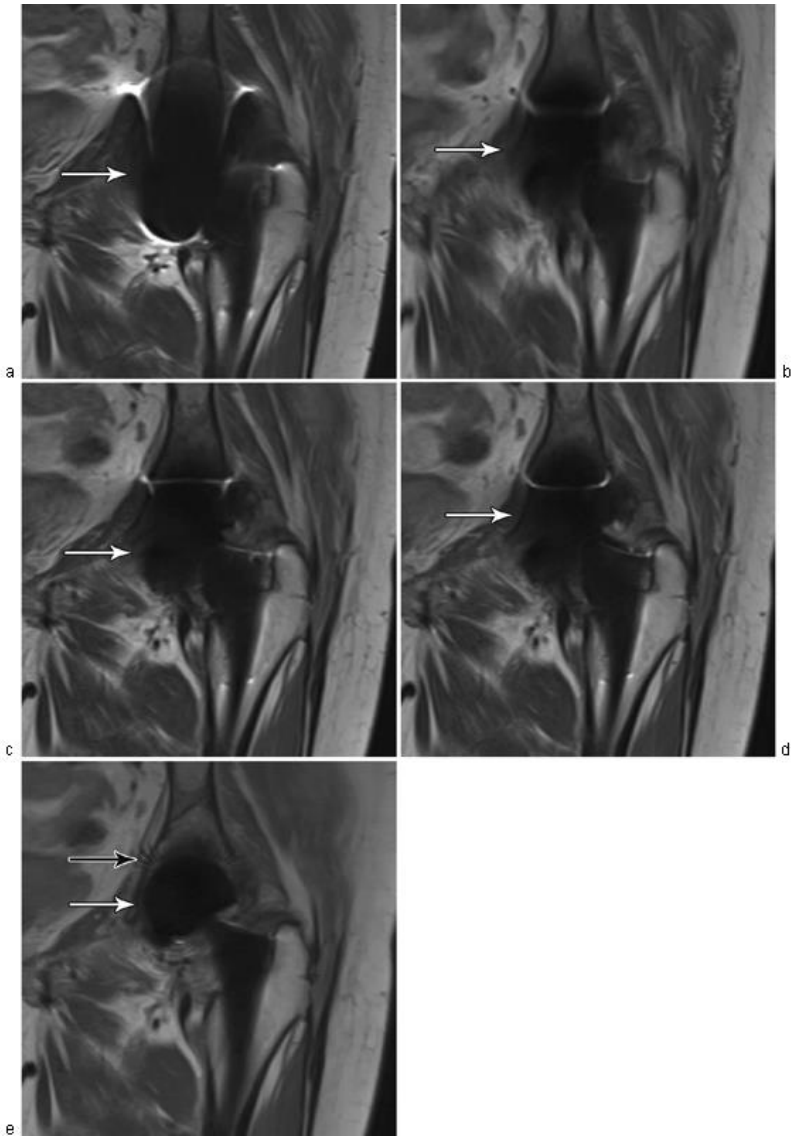

Figure 6 shows the process in optimizing MR images with VAT. The process starts with a generic coronal image (a) with a low receiver bandwidth of 150 Hz/pixel. The next image (b) is an introduction of VAT to the sequence. More of the THA is visible, but the blurring is also present. The next image (c) is with a higher receiver bandwidth of 600 Hz/pixel. The next image (d) has the VAT technique applied to the image. The last image (d) has both in-plane distortion correction and through-plan distortion technic. (32)

The last image in figure 6 is what this experiment strives to achieve for STIR, T2W and T1W images in coronal and transversal planes.

2.3.2 OMAR XD

Slice-Encoding Metal Artifact Correction (SEMAC) relies on a 2D multi-slice TSE sequence that optimizes the through-plan distortions by adding additional phase-encoding steps in the third dimension. It has a small number of phases encodes per slice. By combining the information from all the slice phases encodes SEMAC generates an improved profile. (15)

This technique is challenging because maximizing radiofrequency bandwidths is limited by the maximum radiofrequency amplitude and SAR. For each slice there is formed 3D image by using VAT to avoid in-plane artifacts and phase-encoding in the two other directions which avoids the distortion. The 3D images are then combined for each slice that results in a distortion corrected volume. (31)

The SEMAC technique samples the slice thickness with a phase encoding gradient. The protons with the same phases are combined to diminish the distorted slice. This is seen in figure 7.

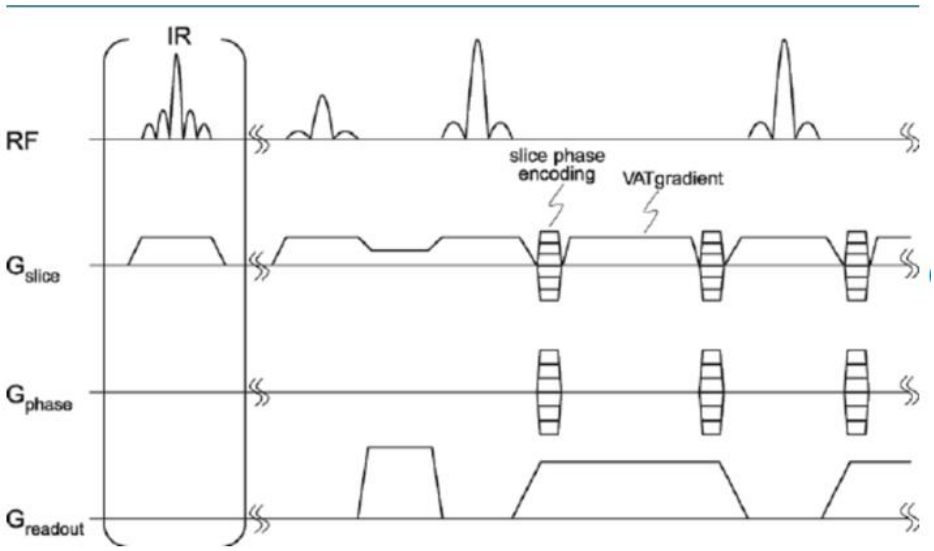

Figure 7 shows a conventional sequence with the through-plane distortion marked with the dotted circle. SEMAC adds a phase encoding in the slice direction, that resolves the distortion of the slices. VAT is also seen in the sequence. (27)

2.4 Specific Absorption Rate

The heating in the tissue is produced from the RF. The scanner is equipped with three operating modes: normal, first-level controlled and second-level controlled modes. The first two modes are

achieved during regular scans, where second-level controlled mode is available in research facilities. These features manage the imaging gradient to manage overheating issues in the patient. This RF exposure is measured in SAR and is the total transmitted power (watts/W) per kilo. SAR is increased with the following: the square of Larmor frequency/B_0, the square of flip angle, the patients size and the number of RF pulses in a given time. (15)

2.5 Compressed Sense

Compressed sensing (CS) is becoming an accessible method, that accelerates image acquisition. CS samples a reduced number of data points and then reconstructs the image with the fewer points and by estimating the missing data point. (15) CS can be added to many sequences, but at present time it is not a commercially available feature with Philips in association with OMAR and OMAR XD.

3. Method and material

This study performed on Philips 1.5T Ingenia with the two most common used THA at the facility. The non-cemented THA is used for patients under 50 years and many patients between 50-70 years of age. The THA choices vary for patients over 70 years old. The non-cemented THA is the primary choice in about 70% of the operations since 2009. (33)

The two THA will be tested in an agar, sterile water and gadolinium mixture. Phantom 1 is a titanium cup and stem consisting of a ceramic Exceed cup with a Biomet “Sirius” stem. This is a cemented THA. Phantom 2 is also a titanium cup and stem consisting of an Exceed ABT cup with a Corail stem. This stem is uncemented. Both arthroplasties are shown in figure 8.

.  (1.)  (2.)

Figure 8 shows THA phantom 1 on the left with a Sirius cemented stem from Biomet, consisting of a titanium. The ceramic external acetabular cup and titanium femoral head are from Exceed. On the right is phantom 2, which is a Corail (DuPuy) non-cemented stem with an Exceed ABT cup consisting of titanium. (34–36)

3.1 Experiment Setup

The phantom experiments are made up of a 2,5% agarose gel containing gadolinium (Gadovist 1.0; 0.1 mmol/L) as seen in figure 9. (37) The water used in this experiment was distilled, so the environment is more controlled. Bobbles were reduced by using a needle to puncture them. Any bobbles were drawn to the periphery of the bucket, where the information was undesirable.

Figure 9 shows the agar powder, 1000 g of destilled water and a bucket the held the THA. Each mixture was poured into the bucket after stirring on a hotplate until boiling.

The mixture is for the first part heated to boiling, consisting of a 2000 g mixture that is set to harden overnight. Then the phantom is placed in the middle of the bucket after carving an indentation for it, so the position of the three individual THA parts were placed as in a patient's body. It is then covered with a headed 1000 g mixture and set to harden again. The phantom was then scanned, but the artifact protruded over the mixtures surface. 1000 g of the agarose mixture was added and set to harden yet again. Each bucket consisted of a THA, 4000 g of an agarose mixture, as seen in figure 10 (1. and 2.). The second part of the phantom experiment was conducted with the same agarose concentration. It was contructed with 2000 g of mixture, with the THA and another 2000 g of mixture. This is seen in figure 10.


(1.)

(2.)

(3)

Figure 10 shows both phantoms (1. and 2.) after a double mixture of agar powder, gadolinium and distilled water. After the gel has set over 24 hours, the gel was fitted with the phantoms and another double mixture was poured over and set over another 24 hours. (38) 3. shows the bucket with the last portion of agarose mixture before it is set aside to harden.

3.2 Phantom experiment sequences

The THAs shown in figure 10 undergoes scanning with the standard protocol consisting of the following sequences: coronal STIR, T2W, T1W and transversal T1W OMAR sequences along with transversal STIR and T2W OMAR XD.

The THA will be oriented so that the implants are aligned with the main magnetic field and as the arthroplasty would be placed, if the patient was in the scanner. (6) The original protocol is viewed as the golden standard. The study will consist of optimized OMAR and OMAR XD for STIR, T2W and T1W in coronal and transversal planes. The phantoms are placed in the center of the scanner with the integrated posterior coil and the anterior coil.

Numerous parameters will be changed to create the optimal solution for these two THA. These parameters are accessible in Appendix (1).

The coronal images of both phantoms were scanned with the golden standard protocol and seen in figure 11.

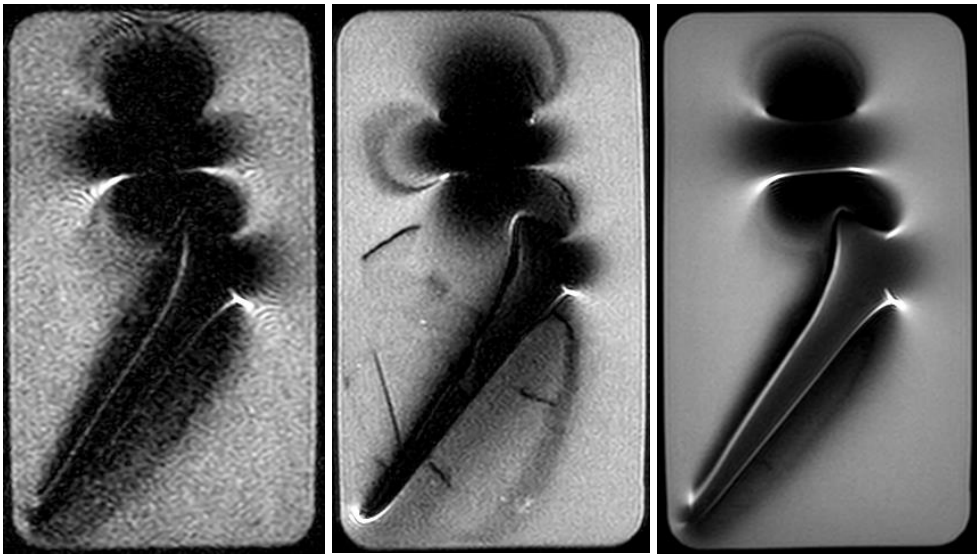
Phantom 1.

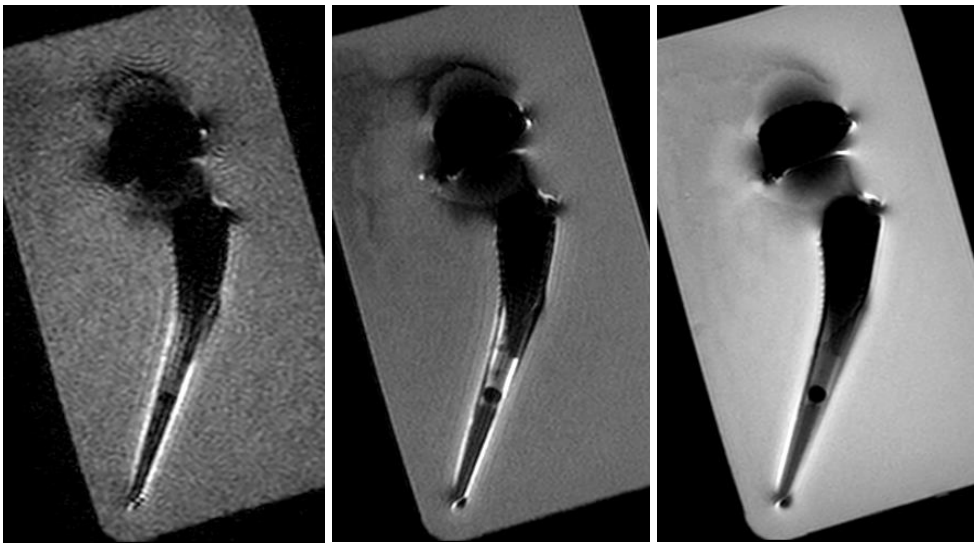
Phantom 2.

Figure 11 shows the coronal images of the golden standard protocol viewed on both phantoms. The sequences are from left to right STIR, T2W and T1W OMAR.

The transversal plan is also scanned in the golden standard protocol. These images are seen in figure 12 for both phantoms.

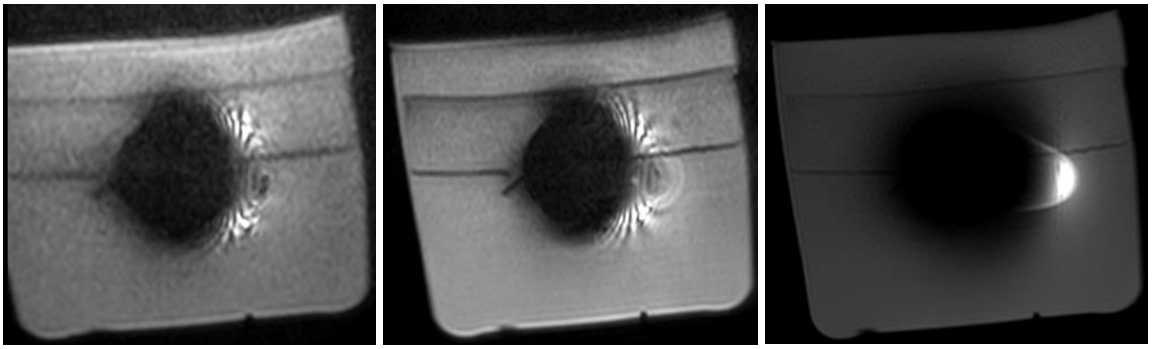

Phantom 1.

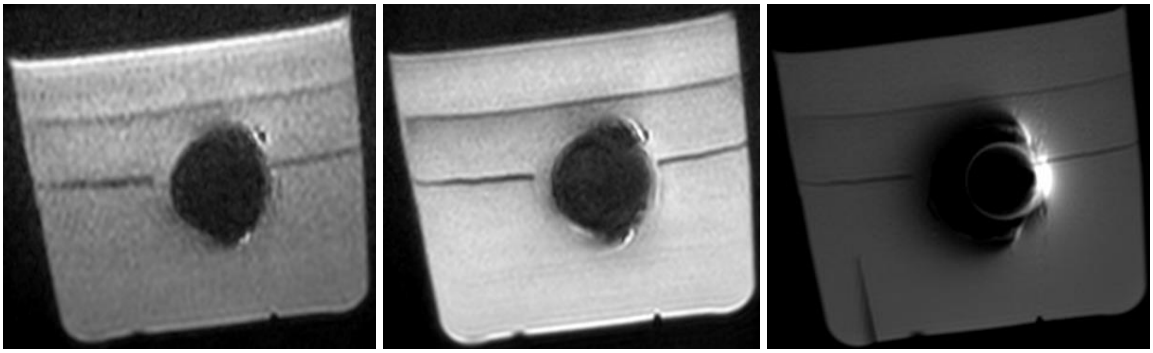

Phantom 2.

Figure 12 shows phantom 1. and 2. in the transversal plan. The sequences are of the acetabular cup on STIR and T2W OMAR XD and T1W OMAR.

The choice was made, to maintain sequences under 10 min., because of the number of sequences (3 coronals, 3 transversals) and the heat to the patient. When Philips introduce CS to OMAR XD the sequence duration may be reevaluated. According to Fritz et al, there are no significant differences between SEMAC and CS-SEMAC, besides the reduction of scan time with CS-SEMAC. (39)

3.2.1 STIR

STIR (Short TI inversion recovery) is spatially nonselective adiabatic inversion pulse that invert magnetization in the desired volume. The sequence is an essential tool to determine fluid in the soft tissue surrounding the hip, because of its ability to invert the signal from lipids. (21)

This sequence is optimized using different parameters, where slice thickness, choice of OMAR vs. OMAR XD, receiver bandwidth, matrix, in-plane resolution and adjusting SENSE is performed in

the following sequences. The golden standard coronal STIR sequences' parameters are available in Appendix (1). It is an OMAR sequences with VAT with slice thickness of 3 mm and a receiver bandwidth of 435 Hz.

In the standard OMAR sequence, the slice thickness is kept small (3mm) along with a short echo train (9). The receiver bandwidth is set at 435 Hz, where it is recommended to be over 500 Hz. This can be one of the indicators for an inefficient sequence or parameter choice. (14) The parameters in table 3 were later changed on numerous levels that can be seen in Appendix (1). Examples of these changes were increased slice thickness to 3,5 mm, where the recommendation for coronal hip scans are between 3-4 mm. (3) The in-plane resolution was increased markedly along with the receiver bandwidth and echo train length to maintain a scan time under 10 min. Two STIR OMAR sequences are seen in figure 13.

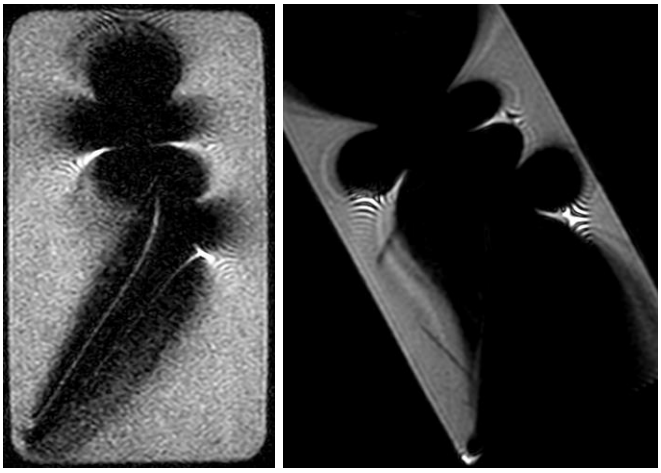

Figure 13 shows the golden standard on the left and an attempt of optimized OMAR with increased bandwidth on the right performed on phantom 1.

Coronal OMAR XD was not present in the golden standard protocol. These were tested and three versions are displayed in table 4.

Table 4 shows Philips' recommended SEMAC on the far left followed by two versions where TR, TE, TI, ETL, NSA, FoV, in-plane resolution and receiver bandwidth are kept as close to each other as possible.

Parameters/Sequences	STIR (SEMAC) Philip	STIR SEMAC 1,7*1,7v	STIR SEMAC 1,4*1,4voxel
Orientation	coronal	cor	cor
O-MAR	SEMAC+VAT	SEMAC+VAT	SEMAC+VAT
Distortion correction	medium	strong	strong
Repetition time (TR) (ms)	2500	2763	2766
Echo time (TE) (ms)	60	60	60
Inversion time(TI) (ms)	155	155	155
Echo train length	15	15	15
Receiver bandwidth (Hz/pixel)	1054,3	1481,7	1218,3
Water-Fat shift (pixels)	0,206	0,147	0,178
Refocusing flip angle (degree)			
Field-of-view (mm2)	250*250	250*250	250*250
Matrix	208*172	148*147	180*179
In-plane resolution (mm2)	0,78*0,78	0,74*0,74	0,63*0,63
Slice thickness (mm)	3,5	5	5
Number of excitations (NSA)	1	1	1
Number of slices	18	19	19
In-plane frequency encoding dir	Right-Left	Right-Left	Right-Left
Acquisition time (min)	07:55	08:34	10:31
SENSE	2,3	3	3

The results of these STIR sequences are seen in figure 14 for both THA phantoms. The slice thickness has increased significantly in order to achieve more signal in the images and keeping the scan time under or as close to 10 minutes as possible.

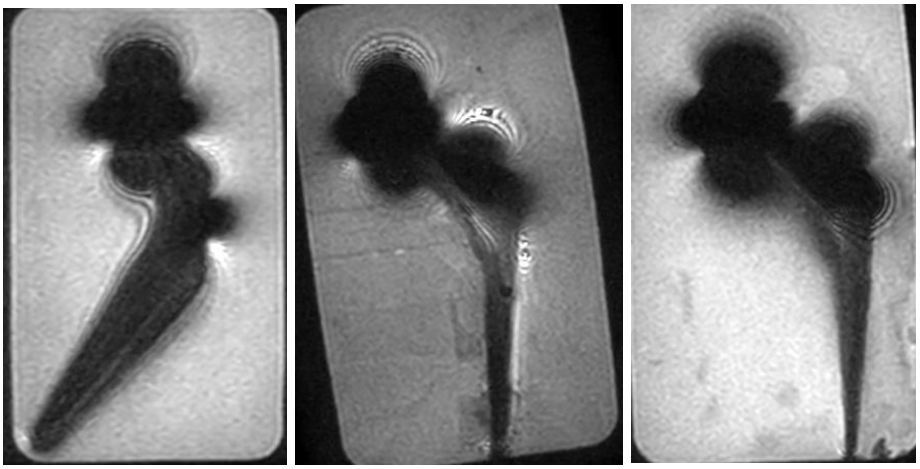

Phantom 1

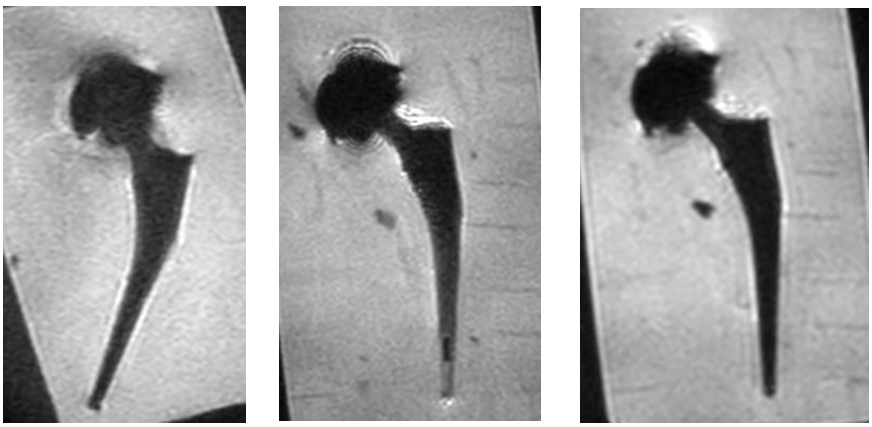

Phantom 2

Figure 14 show the images of the 3 different OMAR XD STIR sequences mentioned in table 4.

3.2.2 T2W

This sequence is equally as important to MR diagnosticians for the sensitivity to fluid collections in the tissue. The long TR and TE leave the tissue bright signaled. (15)

The golden standard T2W sequence is a coronal T2W OMAR sequence and an axial T2W OMAR XD. The parameters are seen for the coronal sequence in Appendix (1) and the images are seen in figure 15.

1.  2.  3. 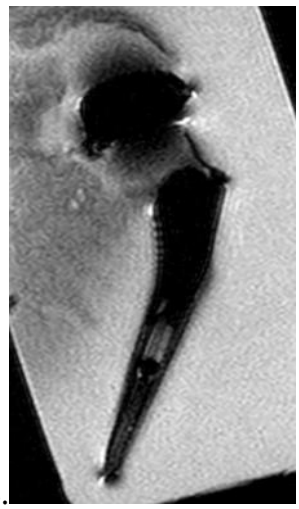 4. 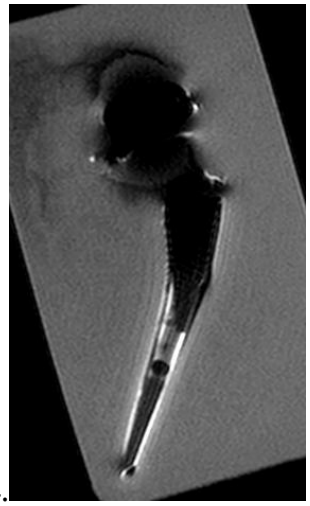

Figure 15 shows the T2W OMAR sequences phantom 1(1. and 2.) and phantom 2(3. and 4.).

The OMAR sequence has a slice thickness of 3 mm along with receiver bandwidth of 435. The same problems are present for T2W images as well as STIR images. The attempt was then made to optimize the OMAR sequence with reduced TR, in-plane resolution, slice thickness and NSA. The receiver bandwidth was kept the same. The slice thickness was increased in both sequences and the FoV in the last sequence was increased along with the number of excitations.

The transversal sequences where also optimized. With both OMAR and OMAR XD along with transversal and alpha angle orientation. T2W sequences with parameters very similar to each other, but with a decrease of slice thickness from 4 mm to 3,5 mm in the OMAR sequence. The purpose was to angle the scan direction to accommodate the THA in a slightly different orientation if this would be a better scan plane. These images were not included for other than subjective image evaluation.

3.2.3 T1W

This sequence is necessary as a counterpart to both STIR and T2W images. The TR and TE are short and produce quit good contrast in the images. Static fluid is viewed dark on this sequence, where fatty tissue is brighter. It is another foundation for MR images and aid in visualizing anatomical structures and their boundaries. (15)

T1W and intermediate weighted sequences as proton density (PDW) are less prone to large artifact distribution than T2W and fat suppression sequences. (3) The golden standard protocol does not consist of PDW images, none the less they were tested as an alternative to T1W images if the radiologist requires it at a later stage. The parameters for the golden standard protocol are visualized in table 5 along with an optimized OMAR and two different OMAR XD attempts of optimization. The differences between the two OMAR sequences are minimal, with a marginal reduced receiver bandwidth. The two OMAR XD sequences differentiate at the receiver bandwidth and the in-plane resolution. All four scan times are visually increased from left to right. The images of these sequences are shown in figure 16.

Table 5 show both OMAR and OMAR XD for the T1W coronal sequences.

Parameters/Sequences	T1W (std)	T1W SEMAC	T1W SEMAC
Orientation	coronal	cor	cor
O-MAR	MARS+VAT	SEMAC+VAT	SEMAC+VAT
Distortion correction		strong	strong
Repetition time (TR) (ms)	500	450	450
Echo time (TE) (ms)	18	10	10
Inversion time(TI) (ms)			
Echo train length	5	4	4
Receiver bandwidth (Hz/pixel)	832,8	1481,7	1218,3
Water-Fat shift (pixels)	0,261	0,147	0,178
Refocusing flip angle (degree)	100	90	90
Field-of-view (mm2)	250*250	250*250	250*250
Matrix	300*257	148*147	180*174
In-plane resolution (mm2)	0,52*0,52	0,74*0,74	0,63*0,63
Slice thickness (mm)	3	5	5
Number of excitations (NSA)	2	1	1
Number of slices	27	19	19
In-plane frequency encoding dir	Right-Left	Right-Left	Right-Left
Acquisition time (min)	02:54	07:59	09:41
SENSE	1,1	3	3

Figure 16 shows the golden standard OMAR T1W sequences along with two OMAR XD sequences on phantom 1.

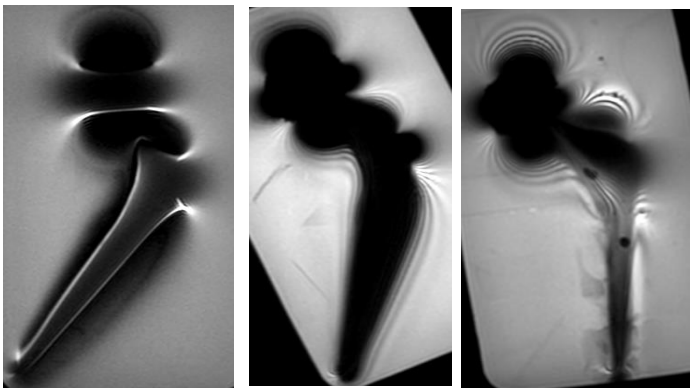

4. Results

The phantom study including the two arthroplasties are evaluated for the image distortion compared to the actual size and with the SNR in the images. This is done to visualize differences between the golden standard protocol and the newer and improved images of both OMAR and OMAR XD. The golden standard protocol was also used as a baseline as the optimized sequences were tested on the healthy volunteer.

4.1 Quantitative analysis of artifact distortion

The artifact volume, that is visable on all the images were measured by one person. This person performed the MR scan, conducted a subjective evaluation of every sequence made. That operator adjusted the sequences with knowledge derived from books, teachings, articles and experience.

Evaluating MR images of the THA for both phantoms are conducted with a subjective method and a semi-objective method. The subjective method is an artifact volume quantification and described intially by Jawhar et al. (40) They used the equivalent measurements by testing knee arthroplasty sequences. They described the method as reliable.

The artifact volume was determined offline using a dedicated picture archiving communication system (PACS) workstation (Philips, The Netherlands) using IntelliSpace Portal, as seen in Appendix (8). The size of the femoral cup is known for both THA. It is also documented on the cup as 48 mm. All the different sequence examples where then measured. For the golden standard protocol, the measurements range from 63.9mm-67mm in the coronal plane and 60mm-76mm in the transversal plane on phantom 1. The same was done on phantom 2 ranging from 51.7mm-54.3mm in the coronal plan and 57.4mm-59.9mm in the transversal plane. The increase in percentage was calculated by the following: $A_{artifact} - A_{prosthesis} / A_{prosthesis}$ or increase/original size * 100%. $A_{artifact}$ is the measured area and $A_{prosthesis}$ is the true prosthesis area. (41,42)

The size increase for phantom 1 is 33.1-39.1% larger than the actual size in the coronal plane and 24.9-58.3% in the transversal plane. The increase in size for phantom 2 is 7.6-13.1% in the coronal plane and 19.5-24.8% in the transversal plane. The goal was to achieve the smallest artifact and the smallest margin between the two different prosthesis'. Table 6 shows the artifact increase for the two prosthesis' for coronal STIR images and in Appendix (4).

Table 6 shows the golden standard coronal STIR on the far left. MARS is OMAR and SEMAC is OMAR XD. The subsequent sequences are the new and optimized STIR sequences. The differences between the two prosthesis' are significant as well as the choice between OMAR and OMAR XD.

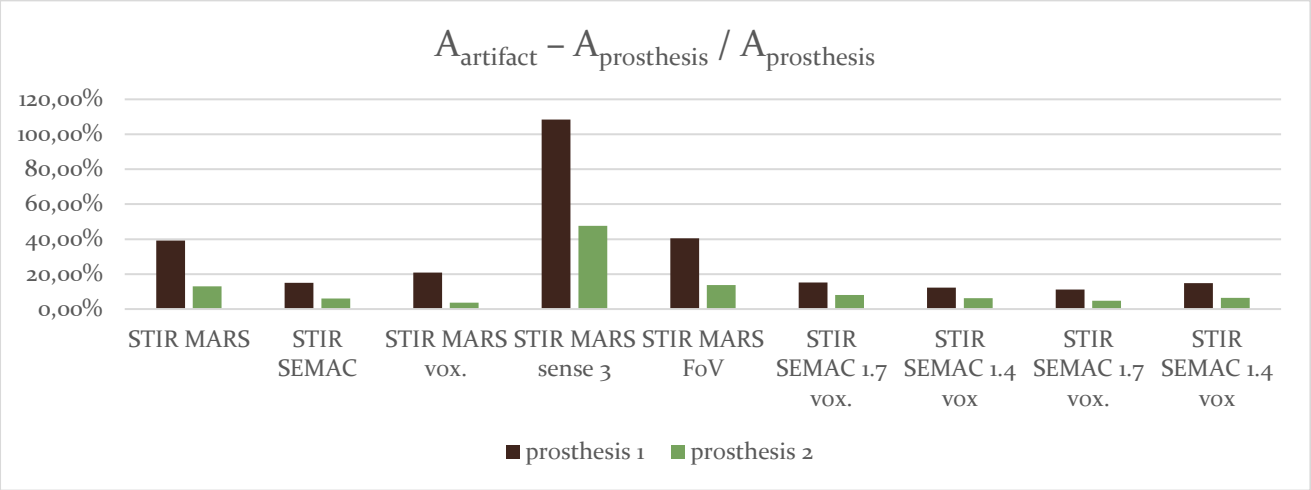

Table 7 displays sequences for coronal T2W images for both THA phantoms.

Table 7 visualize the differences between the artifacts for each prosthesis. The golden standard is at the far left with close to 20% difference between the two THA. Looking at the first SEMAC sequence on the left, the difference between the two prosthesis' are visibly diminished.

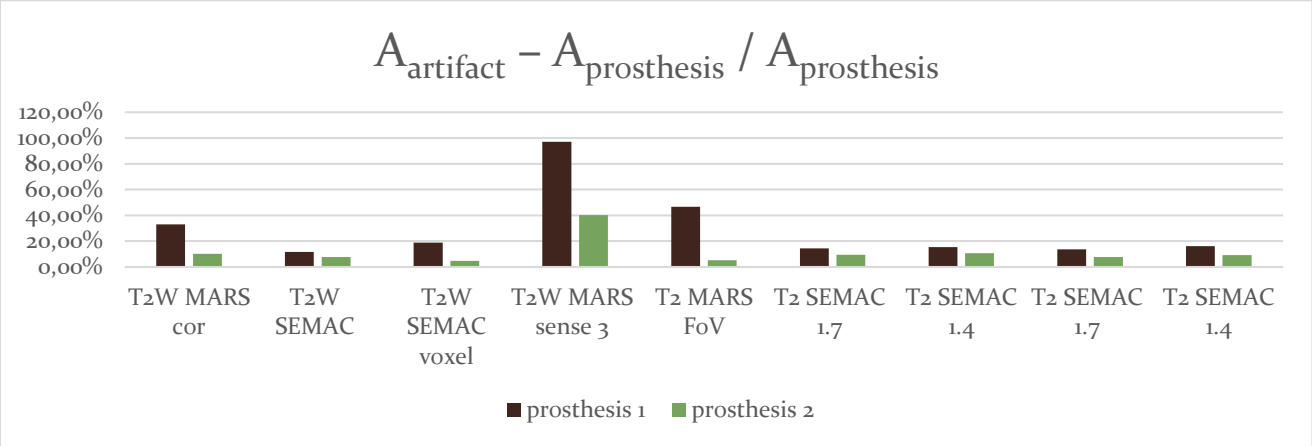

Table 6 and 7 depicts the visible larger artifacts on the OMAR sequences when comparing them to the OMAR XD sequences. There was also a difference between the two phantoms, were phantom 2 showed a significant smaller artifact measurement. The artifact sizes for the coronal T1W is displayed is table 8, with larger measurements when using the OMAR technic compared to OMAR XD.

Table 8 shows large artifacts when using the OMAR technique, which is MARS+VAT. The least artifact distribution is seen using OMAR XD, which is SEMAC+VAT.

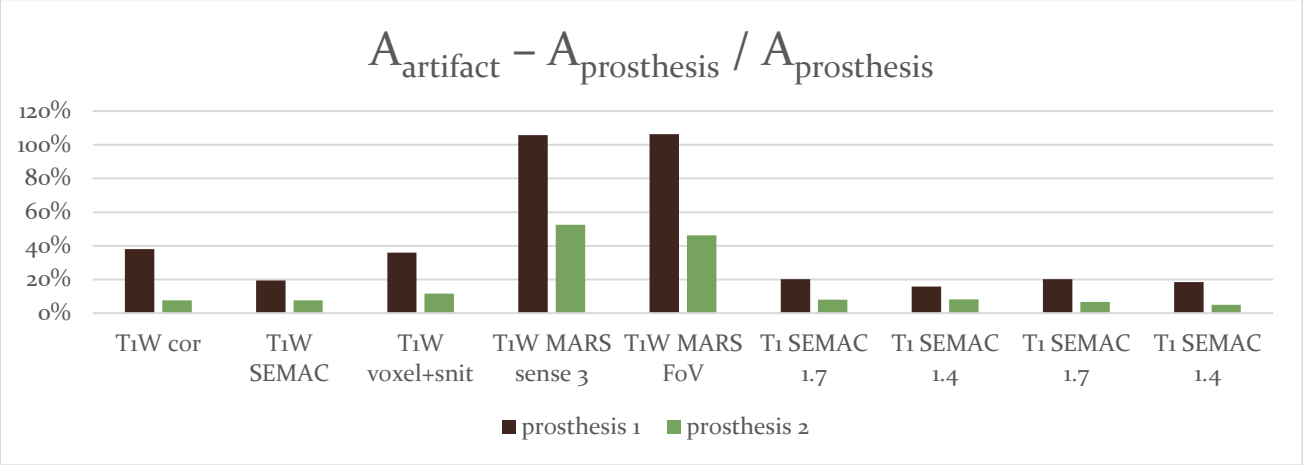

Hips are scanned regularly on 3T. The axial images are often supplemented with axial/oblique slice direction. In the golden standard THA protocol, there are no axial/oblique scans performed. In tables 9-11 there are comparisons for STIR, T2W and T1W between axial and axial/oblique slice direction. These parameters are available in Appendix (1) along with measurements in Appendix (4).

Table 9 shows a significant artifact distortion for prosthesis 1 when using both OMAR and OMAR XD. On the far right there is a negative value (-0.3%) for prosthesis 2. This can be a result of incorrect measurement.

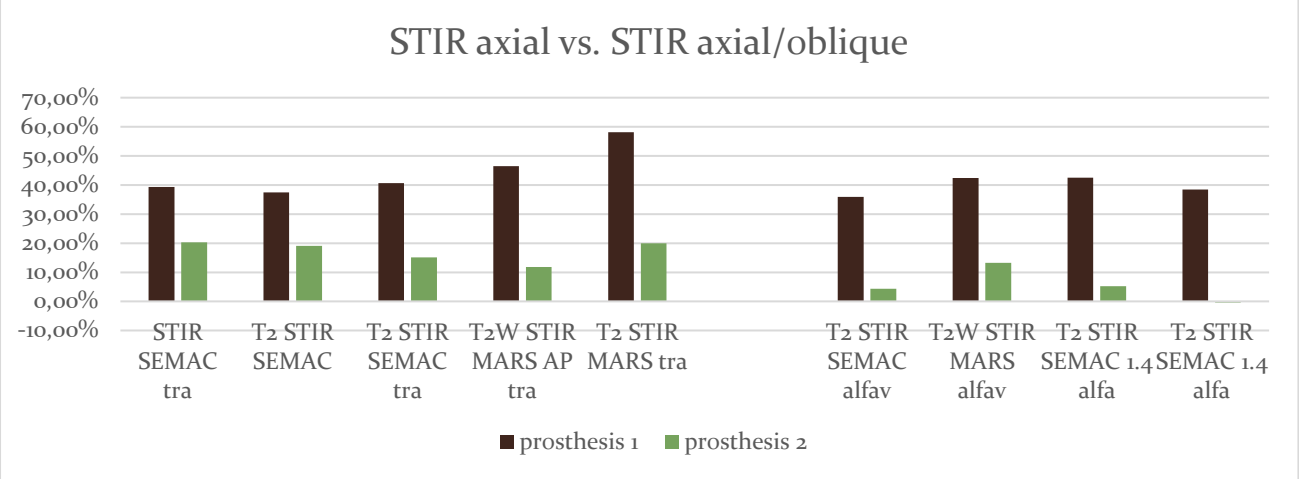

There are significant artifact reductions for prosthesis 2. The seizes for prosthesis 1 are close to similar when comparing transversal and oblique planes.

Table 10 show the large differences between prosthesis 1 and 2, when applying the axial/oblique slice direction. It is also apparent that the OMAR technic is not working out when comparing it to OMAR XD.

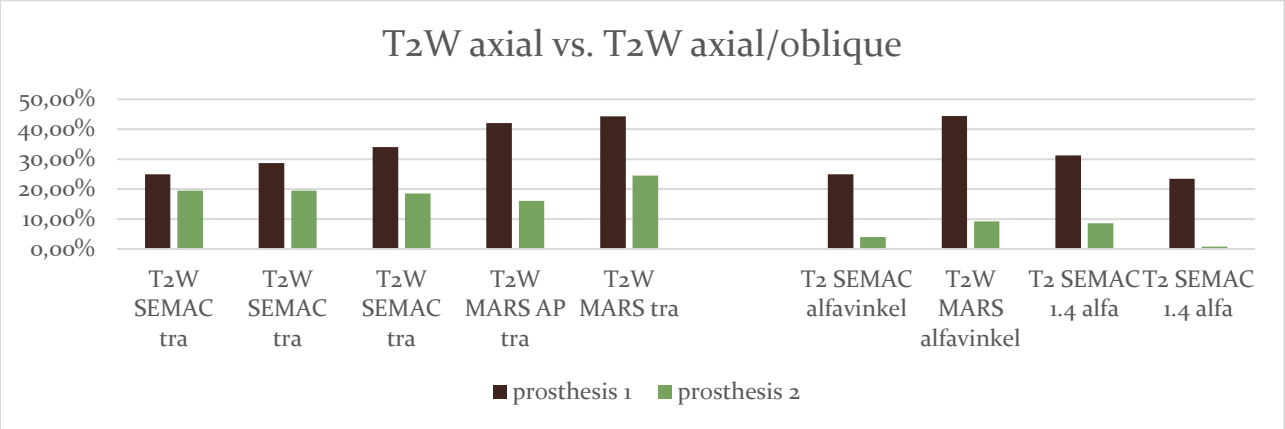

The golden standard transversal T2W sequence is OMAR XD. The attempts of optimization were not an obvious success giving thought to the golden standard version is the better one among the others.

Table 11 show that the golden standard T1W sequence at the far left has the least favorable outcome. This axial T1W sequence is an OMAR technic, which has close to double artifact distortion area than the T1W OMAR XD next to it. The axial/oblique scan direction is favorable for prosthesis 2 as it is for the other sequences.

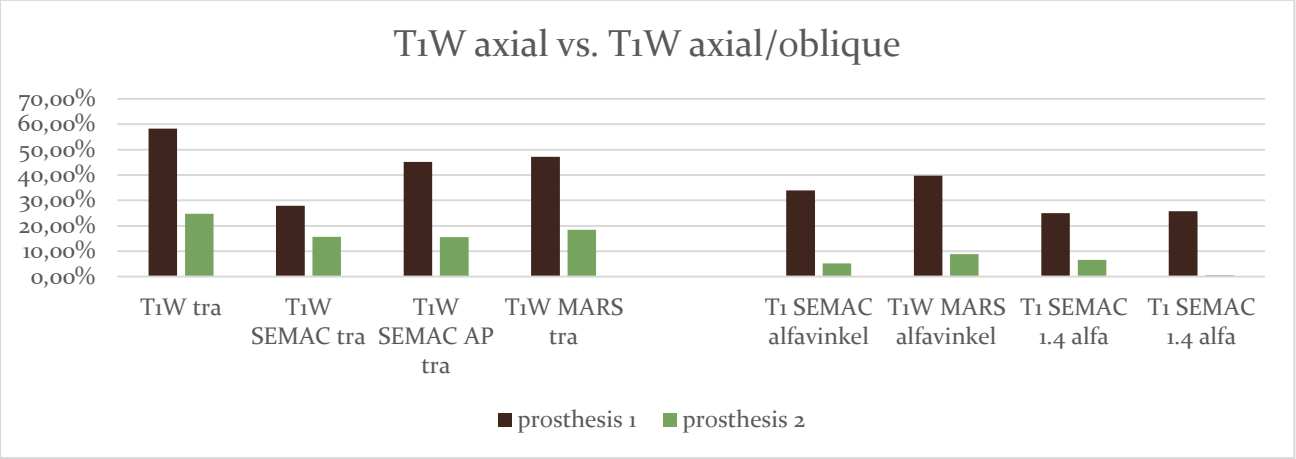

The golden standard transversal T1W sequence produces the largest artifact measurement of all the tested sequences.

4.2 Image evaluation of the prostheses

The sequences were also quantified semi-objectively with the purpose of calculating the Signal-to-Noise Ratio. The definition semi-objective is used, due to the fact, that the Region-of-Interest (ROI) is made for each time the tests were done. They are only able to be the same, when the sequences are in the "same patient" folder. After scanning for 90-120 minutes, the SAR level became too high. A "new patient" was then entered making the ROI's positioning different.

From each center image of the sequences the following data were derived: Area, max., min., mean and standard deviation (SD). Figure 17 is an example of this. The area is as large as the bucket (25345 mm^2), the max. is 2019.6 pixels value range, the min. is 65.9 pixels value range, the mean is 1697.8 pixels value range and the SD is 249.4.

Figure 17 show the ROI as a faint yellow box. This figure consists of the agarose/gadolinium mixture in coronal plane without any phantom in it.

This data is usable in descriptive statistics. The maximum- and minimum-value in each ROI are measurements given with the range of data. The mean is the measures of the central tendency of data. The mean is made up of all the values divided by how many values that are present. SD (σ) shows how the data is spread out. The formula for calculating SD is seen in Eq.7.

$$\sqrt{\frac{1}{N-1}\sum_{i=1}^{N}(x_i-\mu)^2} \quad (7)$$

N-1 are the degrees of freedom (DF), x_i is the data values and μ is the mean. (43) To obtain the signal (S) from all the pixels within the placed ROI viewed in figure 17, the mean signal intensity (I) was determined from Eq.8:

$$S(ROI) = I(ROI) \tag{8}$$

The noise was found by determining the SD of the values calculated pixels. The SNRs for the images are calculated as following Eq.9, (44)

$$SNR(ROI) = \frac{S(ROI)}{SD(ROI)} \tag{9}$$

By using the ROI created in figure 17, the measurements be were calculated for SNR.

The SNR for the agarose/gadolinium mixture in a T2W sequence is seen in Eq.10,

$$SNR(no\ phantom) = \frac{1697.824(no\ phantom)}{249.443(no\ phantom)} \tag{10}$$

SNR $_{(no\ phantom)}$ = 6.8.

This SNR calculation for all the sequences were conducted for both THA phantoms. Attempts were made to optimize the STIR sequence regarding prosthesis 1 to achieve better SNR. They can be seen in table 12 for the coronal STIR sequence.

Table 12 displays the SNR for both THA prosthesis', showing differences between the two along with a markedly low SNR for 2 of the OMAR sequences.

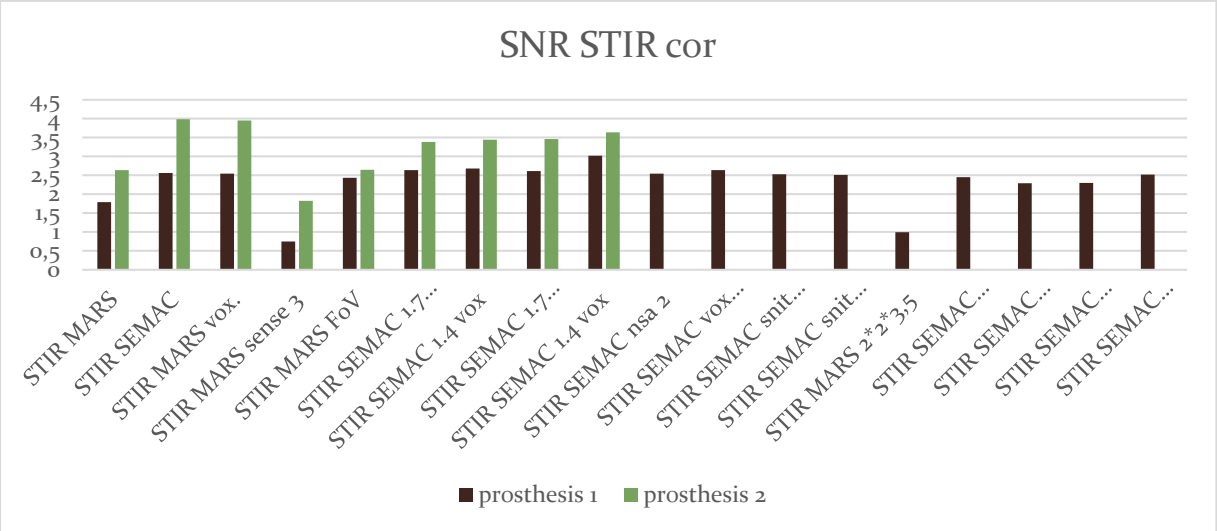

The last 9 sequences were conducted solely on prosthesis 1, because it repeatedly displayed the largest artifact distribution. These last 9 sequences exceeded scan time over 10 min. and were not thought of as sequences in play as a new golden standard sequence. SNR was calculated for all the sequences in the coronal, transversal and oblique planes. Tables 13-15 show the SNR for transversal sequences for both THA prostheses.

Table 13 shows the SNR for the STIR sequences.

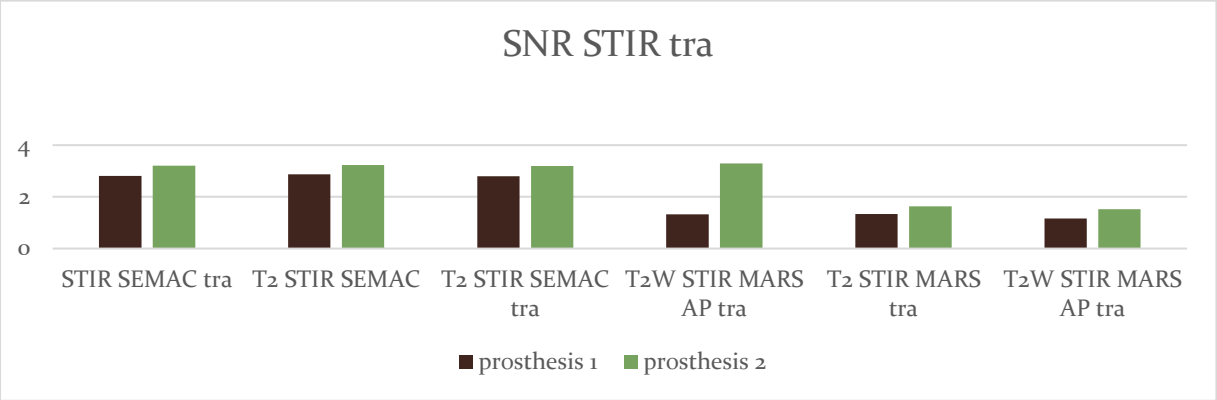

The SNR was lower on all the transversal STIR sequences for prosthesis 1, but OMAR XD was at the forefront when compared to OMAR.

Table 14 were calculations of the SNR for the T2W sequences with both OMAR the three OMAR XD sequences.

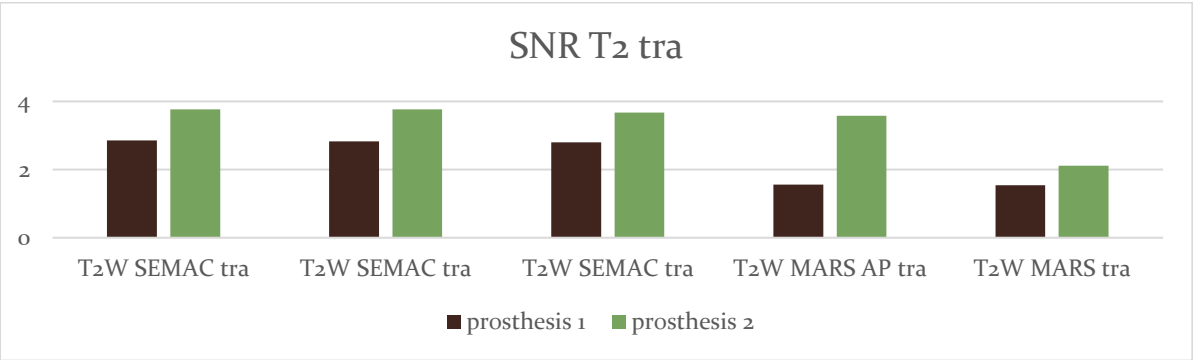

The same result was present on all transversal sequences on prosthesis 1. The SNR is higher on prosthesis 2. This can be seen in Appendix (2).

Table 15 shows the SNR for T1W transversal plan with the golden standard to the far left and attempts of optimized sequences following to the right.

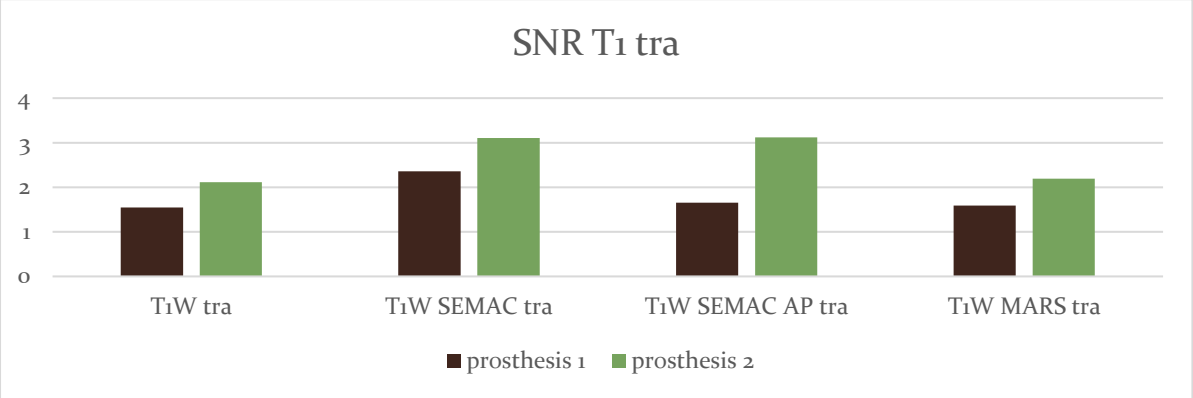

After viewing both the subjective method and a semi-objective method the sequences that displayed the smallest artifact size and the largest SNR from prosthesis 1 was chosen to be tested on the healthy voluenteer.

4.3 Image evaluation of the test patient

The healthy volunteer was scanned with the golden standard protocol followed by the chosen equivalent optimized sequences. The test patient has a Biomet – Ranawat cup and a Ranawat stem. The arthroplasty is not the same as the phantom THA, because the test patient had the arthroplasty put in over 10 years ago. The test patients THA is a non-cemented arthroplasty and is shown on the x-ray in figure 18.

Four observers, with 10-25 years of experience in musculoskeletal MR in interpretation of pathology. They were introduced to a questionnaire that grades anatomical structures near the hip, along with artifacts, image quality and the choice between the golden standard and the optimized sequence. The observers were free to use their preferred sequences hanging along with window and level settings. The questionnaire is viewable in Appendix (10).

Figure 18 shows the test patients hip on x-ray image. This image was not conducted for this study, but because the test patient corresponded with the orthopedic surgeon who needed an up-to-date x-ray.

4.4 Calculating SNR from the test patient

SNR was calculated for muscle, fluid, tendon and fatty tissue. This is managed by the following Eq.11:

$$SNR(ROI) = 0.655 \frac{SI(ROI)}{SD(background)} \quad (11)$$

SI_{ROI} is the mean signal intensity of the three different tissues. $SD_{background}$ is the standard deviation mean from 3 air measurements surrounding the test patient. The 0.655 factor is the Rician distribution of background noise in the image. (45) Tables 16-18 shows the SNR for coronal STIR, T2W and T1W sequences. Appendix (2,3) show SNR as well as CNR.

Table 16 displays the differences between the golden standard coronal STIR sequence and the optimized sequences. The darker color is the golden standard that has lower SNR in each chosen tissue.

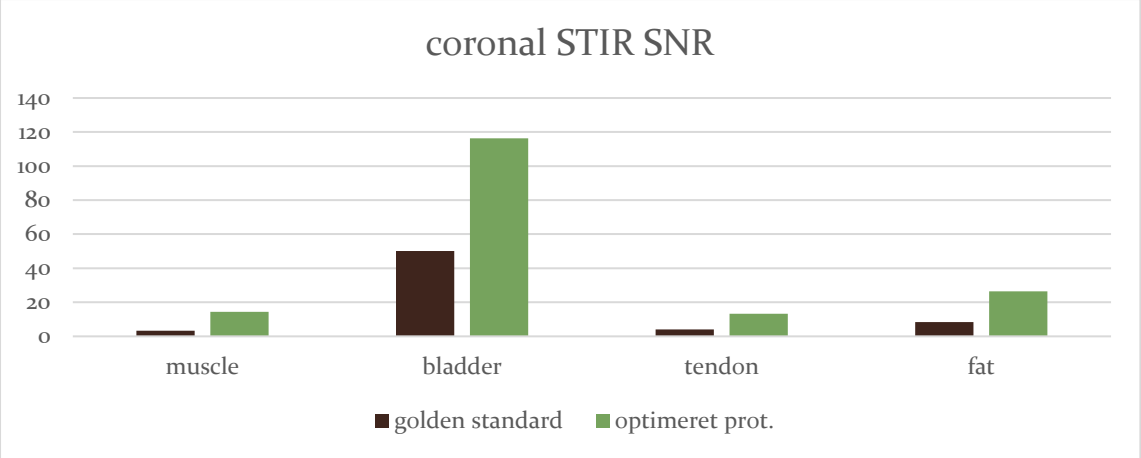

Table 17 shows better SNR for the optimized sequences than the golden standard.

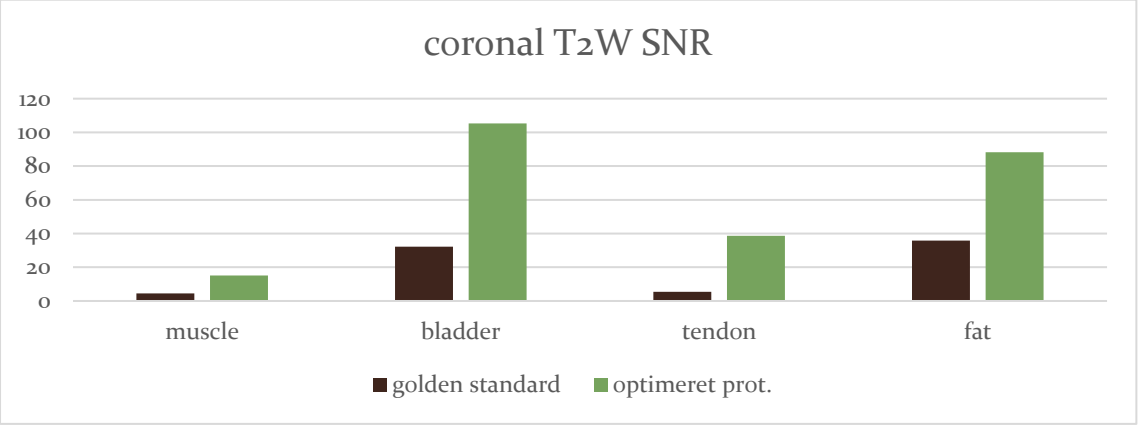

Table 18 shows a distinct difference between the golden standard and the optimized version.

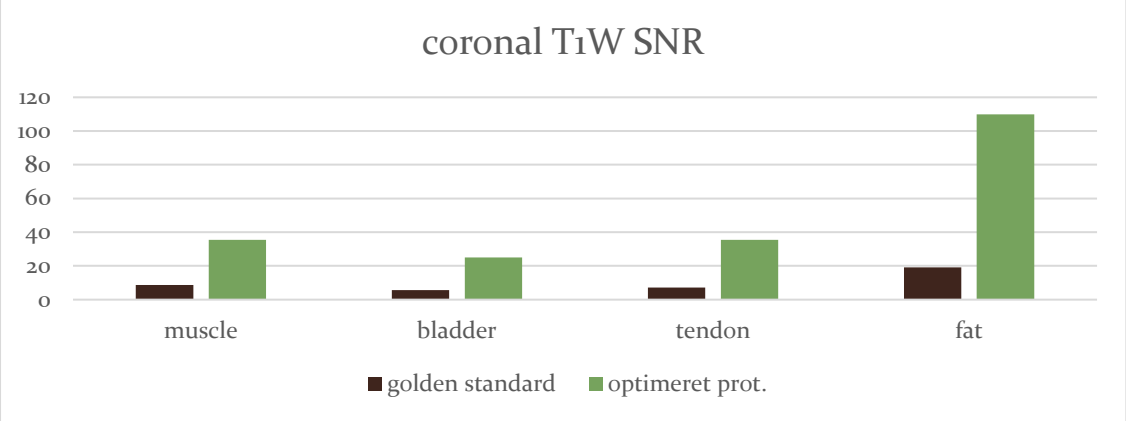

All three coronal sequences from the golden standard protocol was inferior in SNR that has the OMAR XD technic. The same SNR calculations were performed for the transversal sequences. The STIR sequences were close to similar SNR. The T2W transversal sequence shows superiority for the golden standard by an increase in SNR in the tissues. The SNR for the optimized transversal T1W

sequences show a marginally better SNR than the equivalent golden standard version. These tables are available in Appendix (2,3)

4.5 Qualitative analysis of the test patient

The radiologists were asked to rate the images of the healthy test patient with a 5-point Likert scale. The ratings were denoted as following: the lowest rating of 1 is denoted “very bad”/”non-diagnostic”, that indicates a complete obstruction of anatomical details; 2 denoted “poor”/”severe” with substantial obscuration of anatomical details; 3 denoted “adequate”/”moderate” with impairing depiction of anatomical details; 4 denoted “good”/”mild” with minimally impaired, but preserved anatomical details; and 5 denoted “very good”/”none” with unimpaired depiction of all anatomical structures. (39)

The anatomical structures that the observers are asked to view are capsular ligaments, muscles, tendons and vessels in the vicinity of the hip joint. The capsular ligaments are; 1 iliofemoral ligament, pubofemoral ligament; and ischiofemoral ligament. The muscles and tendons are; anterior group 2 rectus femoris muscle, psoas muscle, iliacus muscle, pectineus muscle and sartorius muscle; medial group 3 adductor brevis muscle, adductor magnus muscle and gracilis muscle; lateral group 4 gluteus minimus muscle, glutenus medius muscle, gluteus maximus muscle and tensor fasciale latae muscle; posterior group 5 semimembranosus muscle, semitendinosus muscle and the long head of biceps femoris muscle. The 6 anatomical structure group that the observers are asked to view are the femoral artery and vein. (46)

The radiologists were also asked to view artifacts on the images. The artifact groups were; 7 motion artifacts; 8 Ripple artifacts; 9 edge blurring and 10 fat suppression for the STIR sequences. The last question (11) asked the radiologists to choose between the golden standard sequence and the optimized sequence. (39) One of the filled-out questionnaires is available in Appendix (10). If the anatomical structure were not visible/not imaged, then the cubical is left blank.

4.6 Result of the qualitative analysis

The 5-point Likert scale was applied because of the reliability and to achieve sawed out opinions from the experienced radiologists. The radiologist had the opportunity to choose the extreme options (1; very bad or 5; very good) but also a more granular feedback by choosing the middle point options

(2; poor, 3; adequate or 4; good). By using the 5-point Likert scale, it could point out which areas might need further improvement. The 4 radiologists viewed the images. The center image for the two protocols seen in figures 19-21 are the coronal plane. They were also asked to view the transversal images where only the T1W sequences are seen in figure 22.

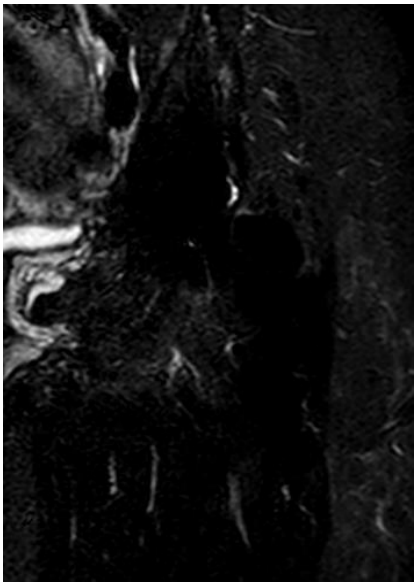

A. OMAR with MARS+VAT technic.

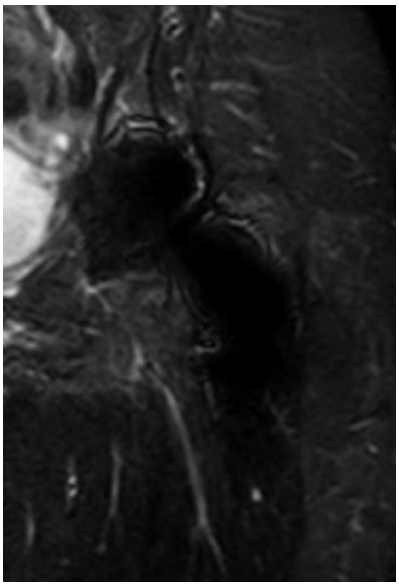

B. OMAR XD with SEMAC+VAT technic.

Figure 19 shows the golden standard OMAR coronal STIR (A) on the test patient and the optimized OMAR XD coronal STIR (B).

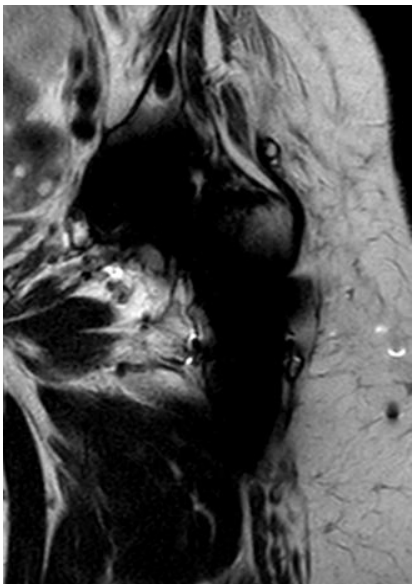

A. T2W OMAR sequence.

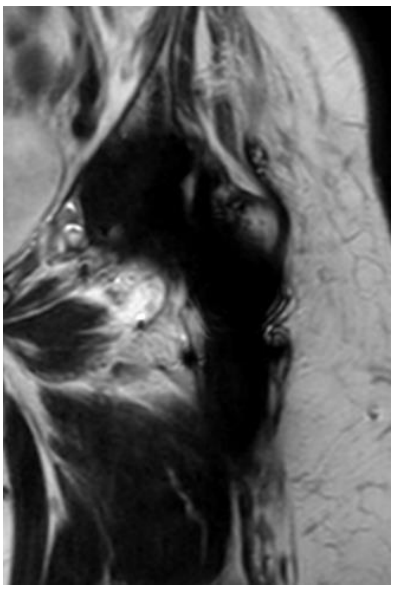

B. T2W OMAR XD sequence.

Figure 20 shows the coronal T2W sequence with the standard protocol OMAR (A) and the equivalent OMAR XD (B).

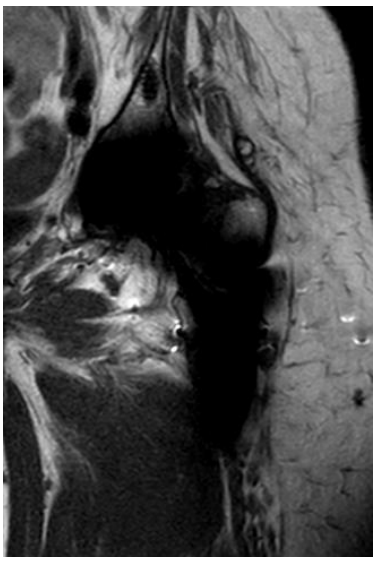

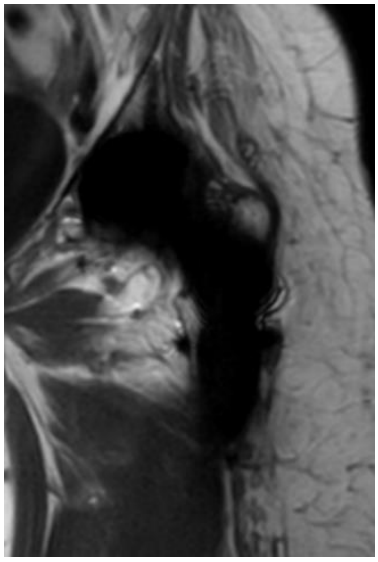

A. T1W OMAR sequence. B. T1W OMAR XD sequence.

Figure 21 shows the T1W coronal OMAR (A) and OMAR XD (B) sequences.

The transversal STIR and T2W sequences were similar in both artifact distribution and SNR for the phantom study. This was also seen on the STIR sequence for the test patient, yet the optimized T2W transversal sequence shows less SNR than the equivalent golden standard version. The optimized T1W transversal sequence has close to 3 times more SNR for the tendon (92.2) and double the SNR for the muscle (40.2) compared to the golden standard (30/24.7). The transversal T1W is displayed in figure 22 for both OMAR and OMAR XD.

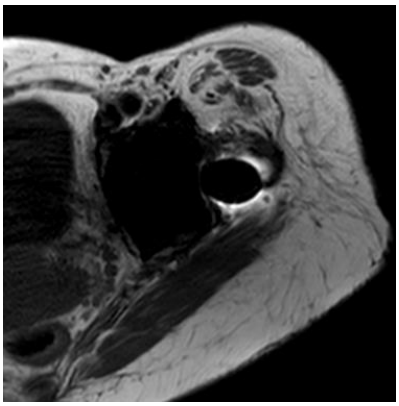

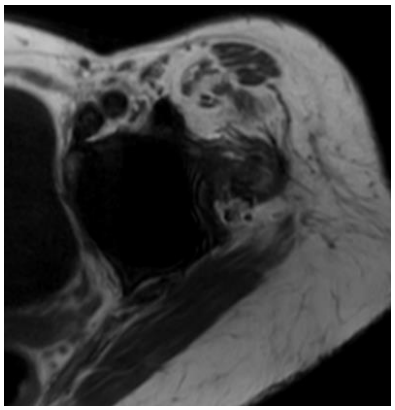

A. T1W OMAR sequence. B. T1W OMAR XD sequence.

Figure 22 shows large signal loss and pill-up on the OMAR technic on image A, where it is not present on the OMAR XD sequence (B).

The test patients THA is measured similarly to the phantom study, but unfortunately the seize of the cup is not known, therefor the size is compared to the other similar weighted sequence. They differ slightly to the phantom study regarding the coronal T2 and T1. Table 19 display the size of the THA artifact of the golden standard protocol and the optimized version for the healthy volunteer.

Table 19 show a larger artifact size for the T2 and T1 in the coronal plane using the optimized sequences. The transversal sequences display a larger difference between the two different protocols, favoring the OMAR XD sequences.

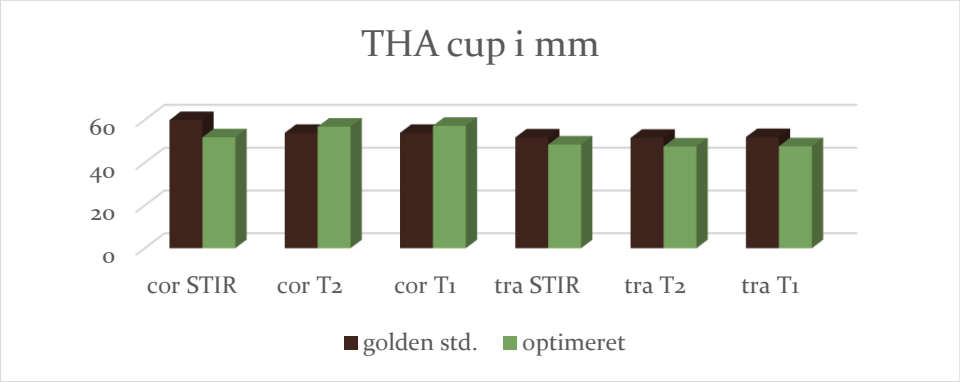

4.7 Calculation CNR

It was possible to calculate the CNR when there were two different tissues present in the image. Paragraph 2.2.3 shows the equation for this. As the SNR has already been calculated, it was possible to use these calculations as following Eq.12:

CNR = [SNR1-SNR2] (12)

where SNR1 was from one type of tissue and SNR2 from another tissue. (39)

The calculations for the coronal STIR, T2W and T1W coronal sequences are shown in table 20-22 and in Appendix (2).

Table 20 show the CNR for the golden standard coronal STIR sequence along with the optimized version.

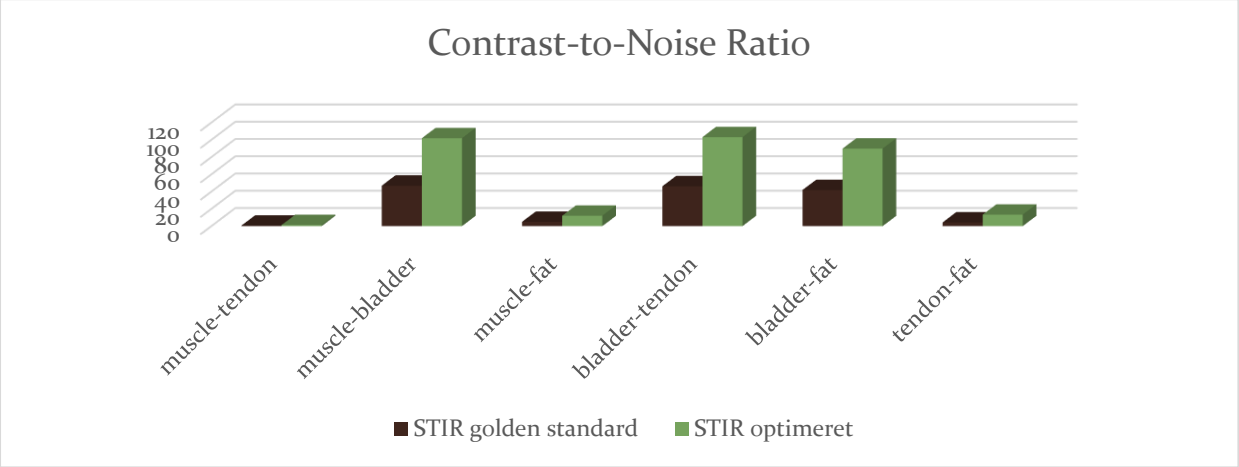

Table 21 show the CNR for the golden standard coronal T2W sequence along with the optimized version.

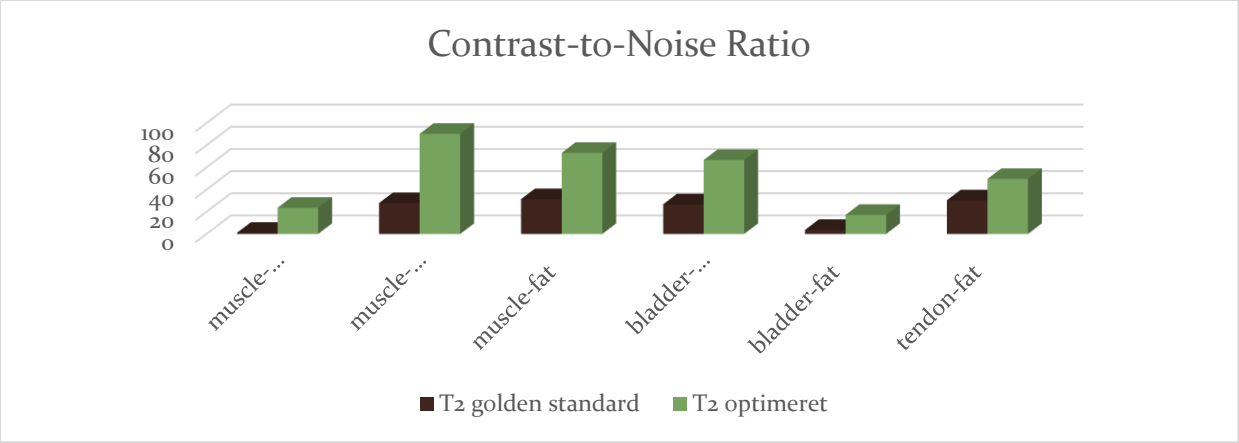

Table 22 show the CNR for the golden standard coronal T1W sequence along with the optimized version.

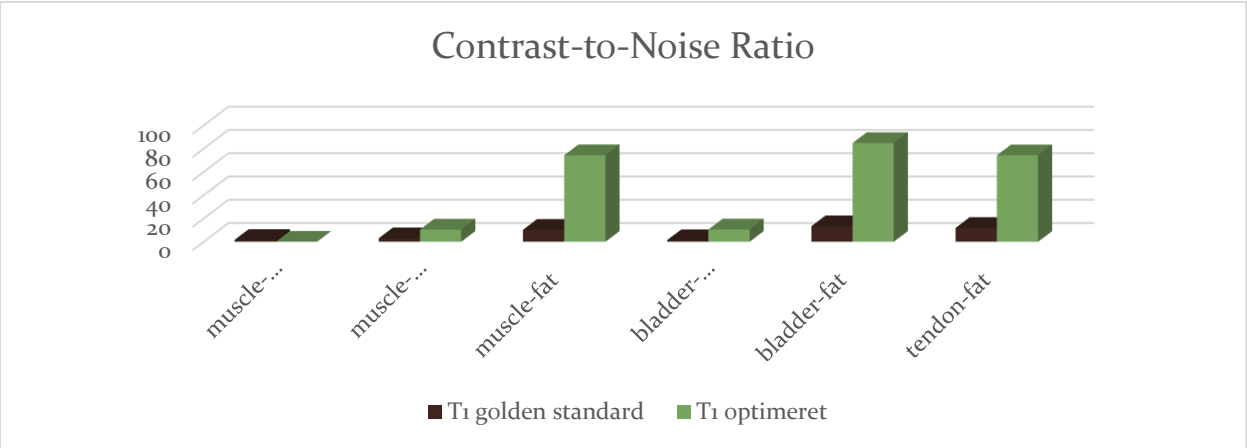

Only the CNR calculations for transversal T1W are shown in Table 23, because the STIR and T2W are very similar. All the calculations are in Appendix (2).

Table 23 show the CNR for the golden standard transversal T1W sequence along with the optimized version.

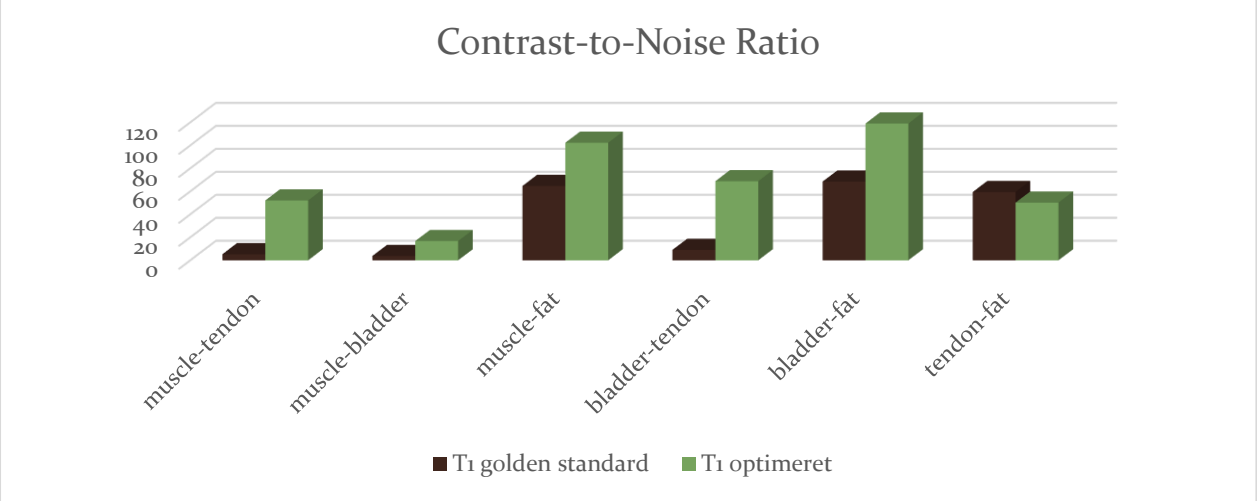

4.8 Statistics

From the 5-point Likert scale there were performed nonparametric tests. Calculations of the median value displays the central tendency best for the Likert scale. It was also possible to calculate the frequencies of responses in percentages along with Chi-squared test and the Kruskal-Wallis test. (47) Sullivan and Artino Jr. offered the perspective of other statistical experts, that debated using parametric tests for Likerts scale when there were at least 5-10 observations per group and these observations were nearly normal. (47)

The responses from the radiologists were inserted in Appendix (5). The statistical software SPSS was also used and documented in Appendix (9). From all four radiologists' answers, calculating the median is used as the measure of central tendency. The Chi-squared tests is used to determine association between the radiologist answers. (47) The Kruskal-Wallis test is performed for the non-parametric data to determine statistically significant differences between more than two groups. It is an extension to the Mann-Whitney U test that compares two independent groups, when the data is not normally distributed. (48)

The data from each radiologist was viewed and compared, where the percentage for each Likert point scale was calculated and seen in table 24 and in Appendix (9). It was notable that there are missing values in the two upper tables and the lower two tables are identical. Viewing the frequencies and percentages, it was visible that the four radiologists may have different approaches to the questionnaire. This made the results of the quality questions visibly subjective. It does not make sense displaying the mean, minimum and maximum.

Table 24 show each radiologist 5-point Likert scale in frequency and percentages.

5-point Likert scale

Value Label	Value	Frequency	Percent	Valid Percent	Cum Percent
non-diagnostic	1,00	20	17,86	18,18	18,18
severe	2,00	21	18,75	19,09	37,27
moderate	3,00	13	11,61	11,82	49,09
mild	4,00	27	24,11	24,55	73,64
none	5,00	29	25,89	26,36	100,00
	.	2	1,79	Missing	
	Total	112	100,0	100,0	

Radiologist 1.

5-point Likert scale

Value Label	Value	Frequency	Percent	Valid Percent	Cum Percent
non-diagnostic	1,00	18	16,07	16,67	16,67
severe	2,00	30	26,79	27,78	44,44
moderate	3,00	24	21,43	22,22	66,67
mild	4,00	15	13,39	13,89	80,56
none	5,00	21	18,75	19,44	100,00
	.	4	3,57	Missing	
	Total	112	100,0	100,0	

Radiologist 2.

5-point Likert scale

Value Label	Value	Frequency	Percent	Valid Percent	Cum Percent
non-diagnostic	1,00	43	38,39	38,39	38,39
severe	2,00	10	8,93	8,93	47,32
moderate	3,00	18	16,07	16,07	63,39
mild	4,00	17	15,18	15,18	78,57
none	5,00	24	21,43	21,43	100,00
	Total	112	100,0	100,0	

Radiologist 3.

5-point Likert scale

Value Label	Value	Frequency	Percent	Valid Percent	Cum Percent
non-diagnostic	1,00	43	38,39	38,39	38,39
severe	2,00	10	8,93	8,93	47,32
moderate	3,00	18	16,07	16,07	63,39
mild	4,00	17	15,18	15,18	78,57
none	5,00	24	21,43	21,43	100,00
	Total	112	100,0	100,0	

Radiologist 4.

It was also possible to categories the Likert scale after each question. SPSS is used for this and these statistics and shown in table 25 and in Appendix (9).

Table 25 shows each question at the top along with the median and the variance.

Statistics

		cap.lig	glut.gr	add.gr	iliops.gr	lat.gr	fem.ves	motion	ripple	edge	fat.sup
N	Valid	44	44	44	44	43	44	44	40	44	16
	Missing	0	0	0	0	1	0	0	4	0	28
Median		1,0000	3,0000	3,0000	1,0000	3,0000	3,0000	5,0000	3,0000	4,0000	4,5000
Std. Deviation		,36205	1,31566	1,47567	1,24974	1,30846	1,00211	1,37998	1,42302	1,42371	,71880
Variance		,131	1,731	2,178	1,562	1,712	1,004	1,904	2,025	2,027	,517

Performing a Kruskal-Wallis test between the 3 radiologists to the 4th radiologist was conducted and shown in table 26. The test is the non-parametric test equivalent to the one-way ANOVA for

parametric values. The test is an extension to the Wilcoxon Rank-Sum test using more than two independent samples. (49)

Table 26 shows the Kruskal-Wallis test where the first three radiologists answers against the fourth radiologist.

Ranks

	radiolog4	N	Mean Rank
radiolog1	non-diagnostic	43	35,95
	Severe	10	43,90
	Moderate	18	58,44
	Mild	16	79,00
	Diagnostic	23	78,43
	Total	110	
radiolog2	non-diagnostic	41	34,09
	Severe	10	48,50
	Moderate	16	53,94
	Mild	17	69,68
	Diagnostic	24	81,50
	Total	108	
radiolog3	non-diagnostic	43	22,00
	Severe	10	48,50
	Moderate	18	62,50
	Mild	17	80,00
	Diagnostic	24	100,50
	Total	112	

A Chi-square test was performed between radiologist number 1 and radiologist number 3. This was also done between the other radiologists. The Pearson Chi-Square values were 67.943, 71.788 and 79.993 between the radiologist, when they were compared to each other. The asymptotic significance for the radiologist were all .000 shown in table 27. These results determine that there was significands between the radiologists' answers and that they were associated to each other. (50)

Table 27 is an example of Chi-Square test between radiologist number 1 and 3.

Chi-Square Tests

	Value	df	Asymptotic Significance (2-sided)
Pearson Chi-Square	67,943[a]	16	,000
Likelihood Ratio	74,348	16	,000
Linear-by-Linear Association	38,948	1	,000
N of Valid Cases	110		

a. 18 cells (72,0%) have expected count less than 5. The minimum expected count is 1,18.

5. Ethical standards

By using a phantom to narrow the possible optimization MRI parameters, it was feasible to scan the THA for an extended timeframe. This would naturally not be an option with the patients as SAR would be increased and result in discomfort for them. The THA study was to prevent the patients from exposure to too high SAR. The test patient had extended knowledge of MR and previously been a test patient numerous times prior. The test patient did not have to have an acceptance from the regional ethics committee. One application was filled in March 2019 and after 90 days (60 day evaluating period) I sent several emails waiting for responses. They replied almost 5 months later that there was no need for any permission to scan a healthy volunteer as this project is furthering the quality of the department. It would be different if the medical journal for the test patient was implicated. If that had been the case, I would have had the task of applying to the Department of Patient Safety under the Danish health law. The documentation to and from the Ethics Committee is listed as Appendix (6,7).

6. Discussion

By applying the knowledge prior to this assignment and the add on theories from books and articles, the OMAR XD could be an automatic choice for the pseudotumor protocol. The golden standard protocol was primarily derived from OMAR sequences with OMAR XD sequences (STIR and T2W) in the transversal plane as the exception.

During the phantom study phantom 1 showed visually larger artifact size than phantom 2. They are both composed of titanium, whereas the artifacts should be close to each other in size. That was not the case, and phantom 1 was primarily used to derived to optimize images.

The phantom study had shown that the SEMAC technic markedly reduce the artifact size in all the sequence attempts tried. This was partly because of the increased bandwidth. Ideally the voxel size should be kept small along with thin slices. The consequence is a decrease in SNR, that can be compensated by increased NSA. The scan time increased the 10 min. cut-off time and therefor slice thickness and voxel size was keep larger than ideal. The slice thickness had in some sequences remained the same and in other sequences, the slice thickness had been increased to obtain more SNR. The cost of higher SNR is reduced image resolution.

Viewing the phantom tests, the largest artifact distribution was 39.2% larger than the original size for the coronal STIR sequence on THA prosthesis 1. The optimized SEMAC technic produced an increase in artifact distribution of 15% to the actual THA cup. The T2W and T1W golden standard sequences had 33.1% and 38% respectably artifacts distribution sizes compared to the actual cup size, where the optimized sequences display an increase of 11.7% and 18.5% artifact distribution. All these measurements were from the cemented THA that showed the largest artifact distribution of the two THA. The optimized sequence performed on the test patient should display superior artifact reduction of all but the transversal STIR and T2W sequences. This is also because the golden standard sequences had the SEMAC technic incorporated. Many parameters were changed and comparing each sequence to each other proved impossible, as too many factors were in play.

The SNR was markedly lower on all three golden standard coronal sequences. When looking at the transversal sequences, the golden standard sequences are superior to the optimized sequences. The SNR was superior in all three SEMAC sequences when looking at the tendon and muscle for the optimized sequences. The transversal STIR was very similar in SNR values between the two sequences 46.2 (tendon) and 18.1 (muscle) vs. 50.7 (tendon) and 13.1 (muscle). There were significant differences between the SNR for the T2W and T1W transversal sequences. The T2W had superior SNR for the golden standard sequence 152.5 (tendon) and 86.6 (tendon) compared to the optimized sequence. The opposite is determined for the T1W transversal sequences where SNR for the golden standard protocol was 30 (tendon) and 92.2 (tendon) for the optimized sequence. Higher SNR in numbers do not account for the overall image evaluation. Artifact distribution could be viewed equivalent to image resolution.

The CNR for the tissues were higher on also all measurements when the coronal sequences where viewed side-by-side. This could be and argument, that the optimized sequences were “better” than the golden standard. The artifacts are reduced with compromise of the resolution in the images. SNR and CNR are merely measurements and the subjective evaluation the radiologist applies determine the choice of sequence. Their knowledge and evaluation of MR images were subjectively done, but that is one of the foundations of analyzing the images. As there had not been major complaints to the golden standard protocol from the radiologists, it had primarily been an issue from the radiographers’ point of view. It was visible that artifacts could be reduced by using OMAR XD or SEMAC technics, but by doing so compromising the resolution.

The 5-point Likert scale provided more leisure to evaluate the radiologist separate and combined evaluation of the golden standard protocol sequences compared to optimized sequences. They were asked to view the images for quality and visibility of anatomical structures with their diagnostic capabilities. Some difficulties arrived with the question- choice and how they were interpreted by the radiologists. They may not be familiar with terminology used by radiographers and vice versa. Viewing the anatomical structures may be unimportant in the greater good, but these structures and common structures for hips MR imaging without a THA. Motion artefacts are seen in the bladder, but it did not have any importance for the THA. The Likert scale does not indicate the correct answer, if the question is not very specific. To achieve that each radiologist could be interviewed separately for further depth. The department have between 4 and 8 radiologists employed to view musculoskeletal MR. The Likert scale can be used to see each radiologist individual views and compared to the other radiologists, but the purpose was to achieve optimal images for future patients.

Performing statistics of the result of the Likert scale resulted in each outcome for the Chi-Square test, that the radiologist’s answers were associated to each other. The statistics were not as predominate in the Chi-Square test results. It was more interesting to view how each radiologist choose to grade the anatomy and image quality in the Likert scale. Radiologist number 1 had a higher percentage of “mild” and “none/diagnostic” answers and fewer “non-diagnostic” answers than any of the 4 radiologists. Radiologist 1. was the only one of the four participants that favored the golden standard protocol. The other three preferred the coronal STIR OMAR XD to the equivalent OMAR sequence. Two of the radiologists confessed to filling out the Likert scale together. One radiologist received assistance from a less experienced radiologist to use the IntelliSpace Portal program and filling out the Likert scale. The radiologists in the department are known for their combined MR image assessment. If they have difficult- or challenging cases, they often combine their knowledge and view the images together giving the patients a quality image assessment.

OMAR XD could at this stage not be implemented with CS, but when that will be accessible, it may reduce the scan time for the sequences without compromising the resolution according to additional articles.

7. Conclusion

The golden standard protocol was only partially implemented with the SEMAC technic. The coronal sequences include the MARS with VAT technic. After conducting the phantom THA tests, it was apparent that all the coronal sequences had markedly larger artifact distribution and lower SNR calculations when compared to SEMAC. The optimized sequences that had the smallest artifact distribution for phantom THA number 1 was then applied to the test patient.

The cemented phantom number 1 distributed the larger artifact of the two test hips. The SNR and CNR are superior in all three coronal sequences and the transversal T1W sequence applied on the test patient. This could be an indicator, that OMAR XD could be implemented for all the scanned sequences for patients under investigation for pseudotumors. The data collected from the radiologists did not indicate that major changes should be made from the golden standard. Even with the larger artifact distribution, the 4 radiologists accept the golden standard sequences. It was possible to achieve images with reduced artifacts, unfortunately that was at the cost of resolution and extended scan time. The artifact distribution is markedly different from each THA phantoms and the healthy volunteer.

The test patient had a different THA than the two tested arthroplasties. The new optimized protocol strived to compensate for artifact reduction, unfortunately that was not optimal for the radiologists.

The only sequence that can be exchanged from the golden standard protocol was coronal STIR SEMAC. By applying this change, the pseudotumor protocol will consist of three OMAR and three OMAR XD sequences.

8. Rights and Publication plans

The data will be collected by me and stored on an external hard drive and locked in a cupboard every day. The order of authors will be: Radiographer Tina Vincens Sørensen, OUH, Radiographer Ph.d Bo Mussmann, OUH, Radiologist Trine Torfing, OUH, and Professor Henrik Bo Larsson, Functional

Imaging Unit, Dept. of Clinical Physiology, Nuclear Medicine & PET, Rigshospitalet, Glostrup, Denmark Odense University Hospital and NTNU.

9. References

1. Walde T, Weiland D, Leung S, Kitamura N, Sychterz C, Engh CJr, et al. Comparison of CT, MRI, and radiographs in assessing pelvic osteolysis: a cadaveric study. Available from: https://www.ncbi.nlm.nih.gov/pubmed/16056041

2. Overgaard S, Ovesen O, Penny J, Ulrich-Vinther M, Stürup J. Metal on Metal (MoM) [Internet]. Available from: http://www.ortopaedi.dk/fileadmin/nyhedsbrev/nov2010/Final_MoM_adhocudvalg_27-okt-2010.pdf

3. Jungmann PM, Agten CA, Pfirrmann CW, Sutter R. Advances in MRI around metal. J Magn Reson Imaging. 2017 Oct 1;46(4):972–91.

4. MRI arthrogram hips stir coronal image [Internet]. [cited 2018 Mar 14]. Available from: https://mrimaster.com/PLAN%20ARTHROGRAM%20HIP%20stir%20cor.html

5. Soft tissue evaluation in patients with Metal-on-Metal (MoM) hip prosthesis [Internet]. [cited 2018 Mar 14]. Available from: http://clinical.netforum.healthcare.philips.com/us_en/Explore/Case-Studies/MRI/Soft-tissue-evaluation-in-patients-with-Metal-on-Metal-(MoM)-hip-prosthesis

6. Orthopedic metal artifact reduction in MRI [Internet]. 2019 [cited 2018 Mar 14]. Available from: http://clinical.netforum.healthcare.philips.com/us_en/Explore/White-Papers/MRI/Orthopedic-metal-artifact-reduction-in-MRI

7. Daniel J, Holland J, Quigley L, Sprague S, Bhandari M. Pseudotumor associated with total hip arthroplasty. JBJS [Internet]. Available from: https://journals.lww.com/jbjsjournala/Abstract/2012/01040/Pseudotumors_Associated_with_Total_Hip.12.aspx

8. Sutphen S, MacLaughlin L, Madsen A, Russell J, McShane M. Prevalence of Pseudotumor in Patients After Metal-On-Metal Hip Arthroplasty Evaluated with Metal Ion Analysis and MARS-MRI. J Arthroplasty [Internet]. Available from: https://www.ncbi.nlm.nih.gov/pubmed/26253484

9. Boas R de MSV, Madeira IA, Lopes AA, Paiva EB, Rodrigues AS. Inflammatory pseudotumor of the hip: a complication of arthroplasty to be recognized by the radiologist. Radiol Bras. 48/2015.

10. Metal Artefact Reduction | Revising MRI [Internet]. [cited 2017 Oct 22]. Available from: http://www.revisemri.com/blog/2011/metal-artefact-reduction/

11. Müller G, Lundin B, von Schewelov T. Evaluation of metal artifacts in clinical MR images of patients with total hip arthroplasty using different metal artifact-reducing sequences. Skeletal Radiol.

12. Aboelmagd S, Malcolm P, Toms A. Magnetic resonance imaging of metal artifact reduction sequences in the assessment of metal-on-metal hip prostheses.

13. McRobbie DW, Moore EA, Graves MJ, Prince MR. MRI From Picture to Proton. Second. Vol. 2007. Cambridge;

14. Dillenseger JP, Molière S, Choquet P, Goetz C, Ehlinger M, Bierry G. An illustrative review to understand and manage metal-induced artifacts in musculoskeletal MRI: a primer and updates. Skeletal Radiol. 2016 May 1;45(5):677–88.

15. McRobbie DW, Moore EA, Graves MJ, Prince MR. MRI from Picture to Proton. Vol. 3rd Edition/2018.

16. Hornak JP. The Basics of MRI [Internet]. chapter 11. Available from: https://www.cis.rit.edu/htbooks/mri/chap-11/chap-11.htm#11.8

17. Hashemi RH, Lisanti CJ, Bradley WG. MRI The Basics. Fourth edition. Philadelphia, PA 19103, USA: Wolters Kluwer;

18. Ruan C. MRI Artifacts: Mechanism and Control [Internet]. [cited 2019 Mar 27]. Available from: https://pdfs.semanticscholar.org/0fd7/f487740e926c3f237d28f558a6e3411d0188.pdf

19. de Jong J, Guerand M. Application tips: voxel size, bandwidth and maer-fat shift. [cited 2019 Mar 27];Issue 36-December 2008. Available from: http://incenter.medical.philips.com/doclib/enc/fetch/2000/4504/3634249/3634100/4987812/5025553/5068598/5529620/FS36_Aptip_BW_WFS.pdf%3fnodeid%3d5529294%26vernum%3d-2

20. Qi S, Wu Z-G, Mu Y-F, Gao L-L, Yang J, Zuo P-L, et al. SEMAC-VAT MR Imaging Unravels Peri-instrumentation Lesions in Patients With Attendant Symptoms After Spinal Surgery. Medicine. Volume 95/ April 2016(Number 14).

21. Bernstein MA, King KF, Zhou XJ. Handbook of MRI Pulse Sequences. Vol. 2004. 84 Theobald's Road, London WC1X 8RR, UK;

22. Spatial resolution MRI. In 2019. Available from: https://radiopaedia.org/articles/spatial-resolution-mri-1

23. FSE Parameters [Internet]. 2019. Available from: http://mriquestions.com/fse-parameters.html

24. Yeung J. Spatial resolution MRI [Internet]. Available from: https://radiopaedia.org/articles/spatial-resolution-mri-1

25. Talbot BS, Weinberg EP. MR Imaging with Metal-suppression Sequences for Evaluation of Total Jount Arthroplasty. RSNA. 36/2016.

26. Jungmann PM, Ganter C, Schaeffeler CJ, Bauer JS, Baum T, Meier R, et al. View-Angle Tilting and Slice-Encoding Metal Artifact Correction for Artifact Reduction in MRI: Experimental Sequence Optimization for Orthopaedic Tumor Endoprostheses and Clinical Application. Available from: http://journals.plos.org/plosone/article?id=10.1371/journal.pone.0124922

27. Sutter R, Ulbrich EJ, Jellus V, Nittka M, Pfirrmann CW. Reduction of Metal Artifacts in Patients with Total Hip Arthroplasty with Slice-encoding Metal Artifact Correction and View-Angle Tilting MR Imaging. Radiology. Oct;265/2012:204–14.

28. Metal Artifact Reduction Sequence. In 2019. Available from: http://radiopaedia.org/articles/metal-artifact-reduction-sequence

29. Lee MJ, Janzen DL, Munk PL, MacKay A, Xiang Q-S, McGowen A. Quantitative assessment of an MR technique for reducing metal artifact: application to spin-echo imaging in a phantom. Skeletal Radiol. 2019 May 9;30/2001:398–401.

30. Bandwidth and Image Quality. In 2019. Available from: http://mrimaster.com/technique%20bandwidth.html

31. Hargreaves BA, Worters PW, Pauly KB, Koch KM, Gold GE. Metal-Induced Artifacts in MRI. AJR. 2011 Sep;197/September 2011.

32. Khodarahmi I, Nittka M, Fritz J. Leaps in Technology: Advanced MR Imaging after Total Hip Arthroplasty. Semin Musculoskelet Radiol. 21/2017:604–15.

33. DHR Årsrapport [Internet]. Available from: https://www.sundhed.dk/content/cms/98/4698_dhr-%C3%A5rsrapport-2017-final-til-offentligg%C3%B8relse_071117.pdf

34. Corail Total Hip System [Internet]. Available from: https://www.depuysynthes.com/hcp/hip/products/qs/CORAIL-Hip-System

35. Exceed ABT [Internet]. Available from: http://www.biomet.dk/dk-medical/dk-hips/dk-primary/dk-exceed

36. Sirius Cemented Femoral Hip Stem [Internet]. Available from: http://www.biomet.dk/dk-medical/dk-hips/dk-primary/sirius

37. Jungmann PM, Bensler S, Zingg P, Fritz B, Pfirrmann CW, Sutter R. Improved Visualization of Juxtaprosthetic Tissue Using Metal Artifact Reduction Magnetic Resonance Imaging. Invest Radiol. Volume 54, Number 1, January 2019.

38. Mitchell MD, Kundel HL, Axel L, Joseph PM. Agarose as a Tissue Equivalent phantom material for NMR Imaging. Magnetic Resonance Imaging. 1985 Nov 11;Vol. 4:263–6.

39. Fritz J, Fritz B, Thawait GK, Raithel E, Gilson WD, Nittka M, et al. Advanced metal artifact reduction MRI of metal-on-metal hip resurfacing arthroplasty implants: compressed sensing acceleration enables the time-neutral use of SEMAC. Skeletal Radiol. 2019 Jun 17;45/2016.

40. Jawhar A, Reichert M, Kostrzewa M, Nittka M, Attenberger U, Roehl H, et al. Usefulness of slice encoding for metal artifact cerrection (SEMAC) technique for reducing metal artifacts after total knee arthroplasty. European Journal of Orthopaedic Surgery & Traumatology. 29/2019.

41. Percentage Change | Increase and Decrease. In. Available from: https://www.skillsyouneed.com/num/percent-change.html

42. Månsson S, Müller GM, Wellman F, Nittka M, Lundin B. Phantom based qualitative and quantitative evaluation of artifacts in MR images of metalic hip prostheses.

43. Descriptive Statistics. In. Available from: http://www.ucd.ie/t4cms/Mean%20and%20Standard%20Deviation.pdf

44. Goerner FL, Clarke GD. Measuring signal-to-noise ratio in partially parallel imaging MRI. Med Phys [Internet]. 38/2011. Available from: https://www.ncbi.nlm.nih.gov/pmc/articles/PMC3170395/

45. Measuring SNR [Internet]. Available from: http://www.revisemri.com/questions/equip_qa/measuring_snr

46. Molini L, Precerutti M, Gervasio A, Draghi F, Bianchi S. Hip: Anatomy and US technique. J Ultrasound [Internet]. 14/2011. Available from: https://www.ncbi.nlm.nih.gov/pmc/articles/PMC3558075/

47. Sullivan GM, Artino Jr. AR. Analysing and Interpreting Data From Likert-Type Scales. Journal of Graduate Medical Education. 2013.

48. Lærd Statistics. Kruskal-Wallis H Test using SPSS Statistics [Internet]. Available from: https://statistics.laerd.com/spss-tutorials/kruskal-wallis-h-test-using-spss-statistics.php

49. Zaiontz C. Kruskal-Wallis Test [Internet]. Wordpress; Available from: real-statistics.com/one-way-analysis-of-variance-anova/kruskal-wallis-test/

50. EZ SPSS Tutorials. Calculate and Interpret Chi Square in SPSS [Internet]. Available from: https://ezspss.com/calculate-and-interpret-chi-square-in-spss/

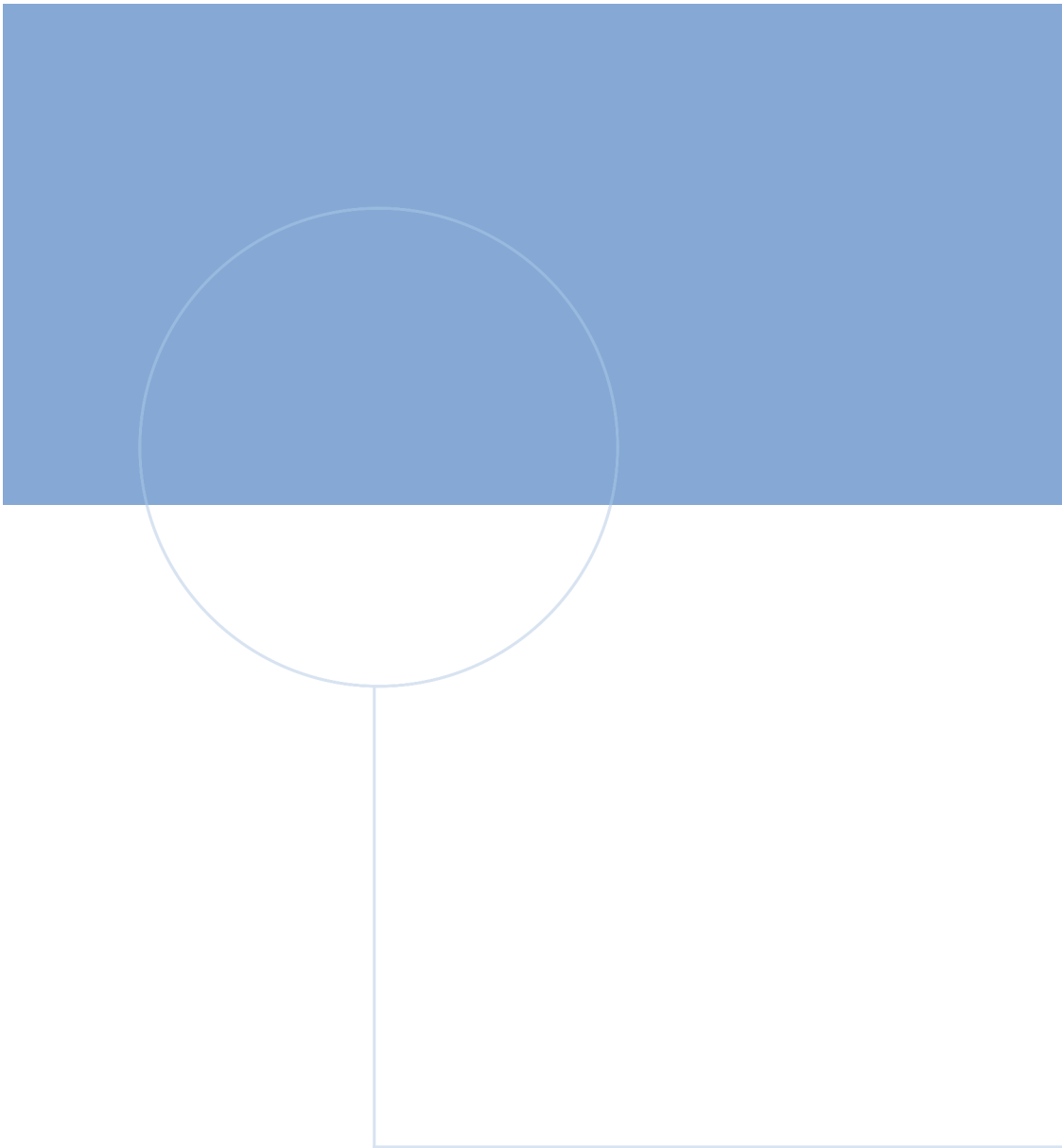

NTNU
Norwegian University of
Science and Technology